U.PORTO

FACULDADE DE CIÊNCIAS
UNIVERSIDADE DO PORTO

Departamento de Química e Bioquímica
Faculdade de Ciências
Universidade do Porto

Third-Order Nonlinear Optical Response of Colloidal Carbon Dots from Femtosecond Z-scan Measurements

Tânia Raquel Mendes Ribeiro

Supervisor: Joaquim C. G. Esteves da Silva

Master Thesis

Master in Chemistry

2015

Page intentionally left blank.

"A poet once said, 'The whole universe is in a glass of wine.' We will probably never know in what sense he meant it, for poets do not write to be understood. But it is true that if we look at a glass of wine closely enough we see the entire universe. There are the things of physics: the twisting liquid which evaporates depending on the wind and weather, the reflection in the glass; and our imagination adds atoms. The glass is a distillation of the earth's rocks, and in its composition we see the secrets of the universe's age, and the evolution of stars. What strange array of chemicals are in the wine? How did they come to be? There are the ferments, the enzymes, the substrates, and the products. There in wine is found the great generalization; all life is fermentation. Nobody can discover the chemistry of wine without discovering, as did Louis Pasteur, the cause of much disease. How vivid is the claret, pressing its existence into the consciousness that watches it! If our small minds, for some convenience, divide this glass of wine, this universe, into parts - physics, biology, geology, astronomy, psychology, and so on - remember that nature does not know it! So let us put it all back together, not forgetting ultimately what it is for. Let it give us one more final pleasure; drink it and forget it all!"

Richard Feynman

Lecture, *The Relation of Physics to Other Sciences*

Page intentionally left blank.

Acknowledgments

I would like to thank to my supervisor Prof. Joaquim Esteves da Silva for receiving me in his laboratory and for his confidence in my work in their different stages.

Dear Prof. Helder Crespo, thank you so much for receive me in your Laboratory (FemtoLab). It was an opportunity that I have no idea how to thank! It was a wonderful experience, it allowed to me to do this work and to have contact with the amazing area of nonlinear optics!

I am also very thankful to all the members of the FemtoLab group (Ana Silva, Cledson Santana, Francisco Silva, Miguel Canhota)! I would like to thank Tiago Magalhães, first for his guidance and assistance in the FemtoLab and for the LabVIEW program that allowed to me to control the Z-scan experiment and acquire data. Let me also thank you for the conversations (and "operations"!) we had, for your enthusiastic manner and your passion for the work, for your constructive criticism, for listening to me and for sharing your interesting views on a number of issues related to this project.

I also thank Dr. Manuel Algarra for the TEM measurements. We are able to see the carbon dots through your "photographs".

I am also using this opportunity to express my gratitude to everyone of the group at REQUIMTE and IFIMUP that I worked with in the area of magnetic nanoparticles during the years of my BSc in Chemistry.

Thanks to my colleagues Sofia Abrunhosa, Diogo Lopes and Daniel Passos.

Finally, I would like to thank to my family.

Page intentionally left blank.

Abstract

A colloidal dispersion of carbon-dots emitting within the green region of the visible spectrum have been prepared and characterized in terms of size and photoluminescence properties. We proposed to study their third-order nonlinear optical response by the Z-scan technique operating with a Ti:sapphire ultrafast oscillator (Femtolasers Rainbow CEP) at a repetition rate of 80 MHz, with a central wavelength of $\sim$ 800 nm. To achieve that, a Z-scan setup was design and built, which is capable to detect the nonlinear refraction and the nonlinear absorption responses of the carbon-dots, simultaneously. A customized program was used to receive and analyze data. Under the experimental conditions used the carbon-dots show both nonlinear optical refraction and nonlinear optical absorption responses. The results showed a mean nonlinear absorption coefficient (β) of about 2.6 cm/GW and a positive nonlinear refractive index (γ) corresponding to a self-focusing behavior. The real and imaginary parts of the third-order susceptibility were calculated from the γ and β values.

This work pretends to be a contribution to the recent investigations of the nonlinear optical properties of carbon-dots and further to understand their suitability to applications in optics, such as optical limiting materials.

Page intentionally left blank.

Resumo

Foram sintetizados pontos quânticos de carbono coloidais capazes de emitir luz na faixa do verde do espectro visível. Este trabalho propõe-se a estudar as suas propriedades ópticas não-lineares de terceira ordem recorrendo à técnica de Z-scan. Nesse sentido foi desenhado e construído um dispositivo experimental Z-scan capaz de medir simultaneamente o índice de refracção não-linear (γ) e o coeficiente de absorção não-linear (β) de materiais. Um programa personalizado foi usado para receber e analisar os dados.

Os pontos quânticos apresentam refração e absorção não-lineares quando iluminados por uma fonte laser de femtosegundos Ti:safira (Femtolasers Rainbow CEP), 80 MHz e comprimento de onda central de ~ 800 nm. Os pontos quânticos de carbono sintetizados apresentam um índice de refração não-linear γ positivo, e um valor médio de absorção não-linear β de 2.6 cm/GW. As partes real e imaginária da susceptibilidade elétrica de terceira ordem foram calculadas a partir dos valores de γ e de β.

Este trabalho pretende contribuir para os estudos recentes sobre as propriedades ópticas não-lineares de pontos quânticos de carbono e as suas possíveis aplicações em óptica, tais como materiais limitadores ópticos.

Page intentionally left blank.

Abbreviations

$\chi^{(3)}$	third-order nonlinear electric susceptibility
γ	third-order nonlinear refractive index
β	third-order nonlinear absorption coefficient
BS	Beam Splitter
CA	Close Aperture
C-dot	Carbon Dot
CEP	Carrier-Envelope Phase
cw	Continuous Wave
DAQ	Data Acquisition
DOS	Density of States
e-h	electron-hole
EEM	Excitation-Emission Matrix
FLS	Fluorescence Spectroscopy
IR	Infrared
NL	Nonlinear
NLA	Nonlinear Absorption
NLR	Nonlinear Refraction
OA	Open Aperture
PL	Photoluminescence
SVEA	Slowly Varying Envelope Approximation
TEM	Transmission Electron Microscopy
TISE	Time-Independent Schröedinger Equation
TPA	Two-Photon Absorption
UV	UltraViolet
UV-Vis	UltraViolet-Visible
XPS	X-ray Photoelectron Spectroscopy

Page intentionally left blank.

Contents

List of Figures

List of Tables

Page intentionally left blank.

Chapter 1

General Introduction

"Dots" are famous for their puzzling but also remarkable optical properties!, and carbon... well, carbon is the "cherished" element of the period table. Together (the carbon-dot) they combine special features like (i) tunable optical properties, such as luminescence, (ii) photostability, (iii) good biocompatibility and low toxicity, (iv) a considerable environmentally friendly nature, among others more or less specific. In what concerns the carbon dots optical characteristics, the part of their nonlinear behavior did not call much attention until recent studies [4, 5]. The versatile family of carbon nanomaterials, namely, carbon nanotubes, nanodiamonds, graphene and including the carbon dots, seems to exhibit a larger third-order nonlinear optical response (i.e. $\chi^{(3)}$ in the order of 10^{-11} to 10^{-13} esu), sometimes exceeding the response of some organic molecules [3, 6]. They can be applied, for instance, as nonlinear optical limiting materials, in optical switching, as saturable absorbers and as optical Kerr lens.

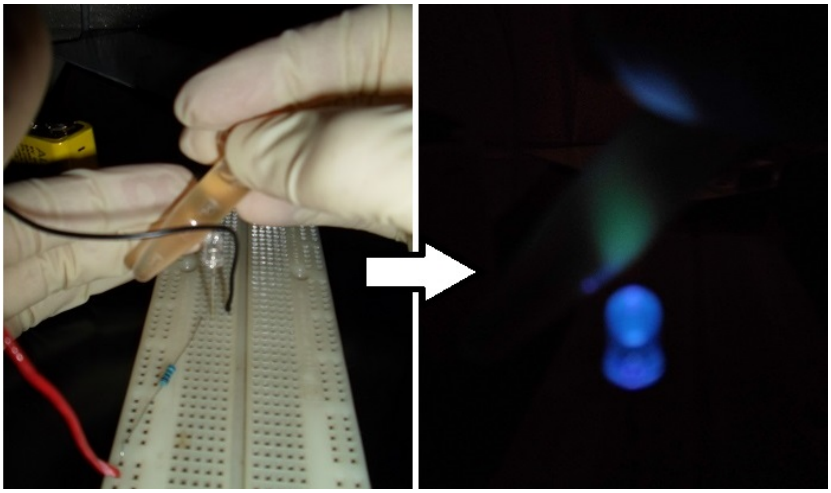

Figure 1.1: Colloidal carbon-dots emitting green light under a purple (365 nm) LED illumination.

The goal of this thesis was to build a Z-scan setup and use it to study the third-order nonlinear optical properties of a self-prepared colloidal carbon dots, using a broadband femtosecond laser. This thesis is structured in the following way. First,

in Chapter 2, we will present carbon dots, the material we intend to study. Then, in Chapter 3, we will present a brief introduction to nonlinear optics. In Chapter 4, we talk about Z-scan technique, from the basic theory (following the approach of Z-scan's developers) to some relevant experimental aspects. A brief review about the application of the Z-scan technique is also presented. After that, in Chapter 5, we introduce the experimental methods for (i) the synthesis and characterization of the carbon-dots, (ii) the construction of the Z-scan setup and (iii) the data treatment. This is followed by Chapter 6, which presents the results and discussions. Finally, in Chapter 7 we present some conclusions and indicate future work.

Chapter 2

Carbon Dots

2.1 Introduction

How small nanoparticles need to be for we to consider them as "dots"[1]? What kind of difference exists between a red color *dot* and a blue color *dot*? To answer this questions we are going to begin from the elementary "particle-in-a-box" problem to transmit the idea of low-dimensional-structure. This quantum confinement approach can be used to explain some properties of *dots* such as their absorption and emission of light. When we are reducing the size so much (in one, two or three dimensions) with respect to the bulk material, we are introducing a restriction in the movement of particles[2] along a crystal lattice [7]. Lets consider the case of one confined dimension. We can deal with a time-independent Schröedinger equation (TISE) for a free particle in a one-dimensional potential well (infinite square well potential):

$$-\frac{\hbar^2}{2m}\frac{\partial^2}{\partial x^2}\psi(x) + U(x)\psi(x) = E\psi(x) \tag{2.1}$$

where $\hbar$ is the reduced Planck constant, m is the particle mass, E is the particle energy and $U(x)$ represents the potential for a rectangular well with the width a and infinitely high walls, which is given by:

$$U(x) = \begin{cases} 0 & \text{for } x \in [0, a] \\ \infty & \text{for } x < 0 \vee x > a \end{cases} \tag{2.2}$$

Whereas inside the rectangular well $U(x) = 0$, equation 2.1 is reduced to:

$$-\frac{\hbar^2}{2m}\frac{\partial^2}{\partial x^2}\psi(x) = E\psi(x). \tag{2.3}$$

[1] Here, the term "dot" will be used to denote the nano-structure only, i.e. independent on the chemical composition. This is because the term "quantum dot" is usually associated to metal contain or semiconductor based dots, such as CdTe. To refer this dots we will use the term - quantum dot. For dots that are mainly composed by carbon atoms we will use the term - carbon dot. The more particular cases will be specified, as graphene dots or nanodiamonds.

[2] i.e. electrons or quasi-particles as excitons.

Rearranging we have:

$$\frac{\partial^2}{\partial x^2}\psi(x) = -k^2\psi(x), \tag{2.4}$$

where

$$k = \frac{\sqrt{2mE}}{\hbar}. \tag{2.5}$$

Applying the boundary conditions ($\psi(0) = 0 \wedge \psi(a) = 0$) to the continuous wave function $\psi(x)$, we get the following:

$$ka = n\pi \Leftrightarrow \frac{\sqrt{2mE}}{\hbar}a = n\pi \quad (n = 1, 2, 3, ...). \tag{2.6}$$

At this point, we reach an important "quantum result", that is a discrete set of allowed energies given by:

$$E_n = \frac{\pi^2\hbar^2}{2ma^2}n^2 \tag{2.7}$$

The solution of equation 2.1 is then a wave function that varies with n:

$$\psi_n(x) = A\sin(\frac{n\pi}{a}x), \tag{2.8}$$

where:

$$A = \frac{\sqrt{2}}{\sqrt{a}}$$

is a normalization constant, since the wave function is treated as a probability distribution, and the probability of finding a particle inside the well is in this case always equal to unit.

Throughout equation 2.7, the energy minimum that the particle can have is:

$$E_1 = \frac{\hbar^2}{2m}\frac{\pi^2}{a^2}. \tag{2.9}$$

Thus, the spacing between neighboring levels are expressed as follows:

$$\Delta E_n = E_{n+1} - E_n = \frac{\pi^2\hbar^2}{2ma^2}(2n + 1). \tag{2.10}$$

In *dots*, particles are confined in all three dimensions. Therefore the quantum confinement situation is alike the case of a particle in a spherically symmetric potential problem. In that case the Hamiltonian of the system is given by:

$$H = -\frac{\hbar^2}{2m}\nabla^2 + U(r). \tag{2.11}$$

Applying the wave function $\psi(r, \theta, \varphi)$ and calculating the eigenvalues we reach the following equation for energy:

$$E_{n,l} = \frac{\hbar^2 \chi_{nl}^2}{2ma^2}, \tag{2.12}$$

where χ_{nl} are roots of the spherical Bessel functions with n being the number of the root and l being the order of the function. These values are listed elsewhere [7]. In fact this discrete sets of energy justifies the alternative name "artificial atoms" given to *dots*. In a simplified analogy, we can think of a as the radius of the *dot*. For a higher a, we will need less energy to excite an electron into the next level (yes, now we can think in levels or at least "sub-bands" instead of thinking in bands, therefore there will be forbiden energy states and the function of density of states becomes discrete - see figure 2.2). Thus, by using the relation $E = h\nu$, where h is the Planck constant and ν is the frequency, we can see that, a photon emission will be redshifted as the radius of the *dot* increases.

So far we talk about structures in which the carriers experienced a quantum confinement due to particle size reduction. Thus, what we meant by "reduction"? Consider λ_e as the Broglie wavelength for an electron, λ_h as the Broglie wavelength for a hole, a_B as the Bohr radius[3] of an exciton. In bulk semiconductors these parameters are considered larger than the lattice constant a_L. However, it is possible to create a structure in which the size is comparable or less than λ_e, λ_h and a_B but stills larger than a_L (see the scheme of figure 2.1). In that structures, the elementary carriers (the excitons) will experience the quantum confinement explored previously. If the wave function becomes more and more confined, we can pass from a weak to a strong confinement (see reference [7]).

$$\begin{cases} \lambda_e \ll a_p \\ \lambda_h \ll a_p \\ a_B \ll a_p \\ a_L \ll a_p \end{cases} \xrightarrow[\text{confinement}]{\text{quantum}} \begin{cases} \lambda_e \geq a_p \\ \lambda_h \geq a_p \\ a_B \geq a_p \quad \begin{matrix} \nearrow \\ \searrow \end{matrix} \quad \begin{matrix} \textbf{weak} \\ a_B \approx a_p \\ \\ \textbf{strong} \\ a_B \gg a_p \end{matrix} \\ a_L \ll a_p \end{cases}$$

Figure 2.1: Scheme for the quantum confinement in low-dimensional-structures, where a_p is the structure size in one, two or three dimensions.

[3] The pair *e-h* that forms the exciton is similar to the hydrogen atom. Thus, the exciton can be characterized by a_B, similar to what happens with the Bohr radius in the Bohr's model of the hydrogen atom.

The density of states (DOS) of the carriers for a d number of dimensions D (1D, 2D and 3D) are represented in figure 2.2. The DOS can be expressed by the relation:

$$\rho(E) \propto E^{d/2-1}. \tag{2.13}$$

For a 0D structure we observe a δ-function-like DOS because of the set of discrete energies.

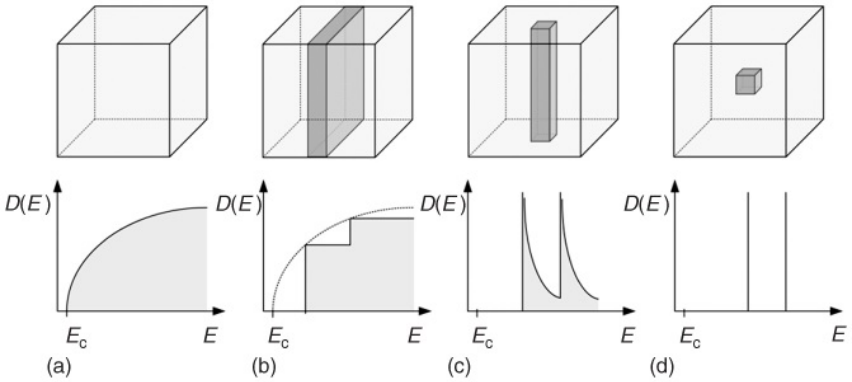

Figure 2.2: Representation of the effect of electronic confinement on the DOS for: (a) bulk material; (b) one-dimensional (1D) confinement - 2D structure called quantum well; (c) 2D confinement - 1D structure called quantum wire; (d) 3D confinement - 0D structure called quantum dot. Reproduced from [1].

These theoretically discrete transitions become approximately Gaussian distributions mainly because of the inhomogeneous broadening. Roughly, the inhomogeneous broadening occur because usually we deal with a distribution of sizes, instead of one unique *dot*.

In the next sections we will address some physicochemical and optical properties of the C-dots, namely, photoluminescence. We will also discuss the fact that the quantum confinement effect seems not to be the only reason behind the process of photoluminescence in carbon based dots.

2.2 Physicochemical Nature

C-dots are almost nearly spherical nanoparticles consisting of an arrangement of a variable sp^2/sp^3 fraction of carbon atoms. Moreover the oxygen content attached to carbon atoms can be relatively high (depending, for instance, of the synthetic route or if the final material is a colloidal dispersion or a thin film). Sometimes, due to the presence of high amounts with sp^2 hybridization, they are called graphitized

C-dots, or due to the presence of high amounts of oxygen they are called carbogenic dots [8]. Just for the reference, there are three possible hybridizations for the carbon atom, namely, sp, sp^2 and sp^3. The hybridization corresponds to the mixture of a $2s$ atomic orbital with one or more $2p$ atomic orbitals (p_x, p_y, p_z) in order to enhance the binding energy of the carbon atom with other atoms in the neighborhood. One $2s$ atomic orbital with one $2p$ atomic orbital form an sp orbital, one $2s$ with two $2p$ atomic orbitals form an sp^2, and so one [9,10]. Depending on the rearrangement and the hybridization of the carbon atom, the C-dot can have sites with high degree of crystallinity and others nearly close to amorphous. The physicochemical properties of graphene-oxide dots seems very close to the C-dots.

2.3 Photoluminescence

Materials can emit light either by luminescence or incandescence. Luminescence can be classified according to the excitation process used [11], as we can see in table 2.1. Moreover, we can find the terminology fluorescence or phosphorescence for luminescence. Roughly, the process of phosphorescence happens in a slower time scale than the process of fluorescence. Here we will only discuss the photoluminescence (PL) of C-dots - that is also called fluorescence.

Table 2.1: Luminescence classified according to some excitation method's

Excitation process due to	**Luminescence Type**
Visible or ultraviolet radiation	Photoluminescence
X-ray radiation	Roentgenoluminescence
High-energy radiation (α, β or γ rays)	Radioluminescence
Electric fields	Electroluminescence
Electron bombardment	Cathodoluminescence
Cation bombardment	Ionoluminescence
Chemical processes	Chemiluminescence
Biological processes	Bioluminescence
Mechanical friction or grinding	Triboluminescence

Dots exhibit photoluminescence within the visible region when illuminated by near UV radiation. The light that is emitted by the *dot* can be tune, in order to achieve different wavelengths of light emission, that will cover the entire visible spectrum. As we saw in the previous section, the color (wavelength of the emitted light from the *dot* during the relaxation process) is strongly related with their size. In the case of quantum-dots (as CdTe or CdSe), the PL arises from the radiative recombination of the carriers - e-h pairs - due to the mechanism to be band-gap in origin. That

band-gap energy is affected by the confinement introduced with the reduction of the material's size. The physical dimension of the particle (nanometer scale) confines the excitons in a manner similar to the "particle in a box" problem presented previously. The result is a quantization of energy levels. Thus, in principle, by changing the size of the particle, we will change the band gap energy and, as a consequence, the emission of light. However, a Stokes shift can occur. In this case one says that PL is Stokes-shifted from the absorvance. That happens for instance because of structure's vacancies or impurities at the surface of the quantum-dot.

The mechanisms behind the PL of C-dots are not yet clear and are still in investigation. The effect of quantum confinement is present and affects the π-domains within the particle - the confined aromatic structures have suitable band gaps. However, it seems not enough to fully describe the PL behavior in C-dots. Experimentally, it seems possible to change the color of a C-dot without necessarily applying changes in their size, but applying in the surface (as surface passivation) [8, 12]. The hybridization of the carbon at the surface and the attached chemical groups makes the surface an additional contribution to PL. On the basis of these assumptions, there are investigations throughout temperature-dependent PL, time-resolved PL, and steady-state PL (i.e. excitation-emission spectra). For more details about this subject we refer the reader to the references [13–16].

2.4 Synthesis

This topic pretends to give the reader a very briefly reference of the many different ways to synthesize C-dots. We will not go into details, since there are many reviews covering the subject in detail (e.g. see references [17–19]).

As usual for nanomaterials, we can synthesize C-dots by a method that belongs to a bottom-up or a top-down approach. If you are preparing your C-dot (or broadly another nanomaterial) using other material(s) as a starting one(s), your method is classified as a top-down approach. On the other hand, if you are synthesizing your C-dot from the beginning (i.e. by chemical reactions) you are using a bottom-up approach.

Starting with bottom-up we have mainly the methods - (i) hydrothermal (ii) microwave-assisted (iii) thermal methods (iii) aqueous based (iv) organic/organometallic precursors based (v) arrested precipitation and (vi) electrochemical based methods. The hydrothermal method [20], for instance, requires an aqueous solution and high temperature (a hundred of Celsius degree) and pressure. As the name suggests if the C-dot is synthesized under microwave irradiation the reader can call it

microwave-assisted. This method is often used when a good temperature control is required. Moreover, for the organometallic based methods three components are usually required: the carbon precursor, the suitable organic surfactants and the organic solvent.

Nanoparticles, graphene or carbon nanotubes, are example of starting materials for a top-down approach. In this case, lithography and laser ablation are the two main methods used to prepare the C-dots.

Chapter 3

Nonlinear Optics

3.1 Introduction

Absorption, refraction, scattering and luminescence... are all examples of "normal" optical effects, that is to say, material's responses that could be described by a linear function of physical quantities. So, a question arises: Under what circumstances this approach fails?

Imagine having a quantity n that can be expressed in terms of a quantity I by the following relation:

$$n = 5 + 3 \times 10^{-11} I$$

Let us say that the reader know the value of the variable I and are interested in find n. If the value of I is 10, what is the value of n? The reader will immediately say 5, neglecting the quantity $3 \times 10^{-11} I$. Suppose now that $I = 10^6$. Maybe this time the reader will say that n is "approximately 5". And if $I = 10^{11}$, what will be the reader's answer? Clearly n remains almost constant for low values of the quantity I and the situation changes when the value of I increases.

Let us call n the refraction index of a material and I the intensity of light (that is proportional to the electric field squared $|E|^2$). We will only be able to detect changes in the refraction when we are using high intensities of light. Otherwise, for low intensities, we will assume that n is a constant. This is the key of nonlinear optics - when we have high values of intensity of light (or irradiance[1]), the circumstances change the usual optical parameters and they become functions of the intensity of light. Only after the birth of lasers we were able to easily achieve so high intensities. Therefore, the area of nonlinear optics is intimately related with lasers - which are coherent[2] light sources with relatively high intensities, when compared to incoherent

[1] "Irradiance" is the power per unit area. It is often called "intensity" without distinction. However, intensity was first defined as the power per unit steradian (symbol: sr). Througouth this thesis the terms intensity and irradiance (I) will be used with the same meaning. With "normal" values of I we mean values of the order of a few W/m^{2}and with high values of I we mean of the order of MW/m^2.

[2] In the case of ultrashort lasers, we speak of highly spatial coherent sources, since they have low

light sources (e.g. lamps). It is common accepted that the observation of the second-harmonic generation in 1961 by Franken et al. [21] marked the birth of nonlinear optics. Since then, the field has been expanding "exponentially"...

We next look at the differences between linear and nonlinear optics and how we can describe nonlinear optical behavior in matter. We will also look at the effects arising from the nonlinearity, specially from the cubic polarization, namely, the optical Kerr effect. The approach for the interaction of light with matter that will be mainly used is that of the classical theory, [22] and the magnetic field of the electromagnetic wave will be neglected. We will not going deep in details. An extended mathematical treatment and details for the following section can be found in references [23, 24]. We will main be following references [22, 25] throughout this chapter. Table 3.1 will be useful to remind the reader of the SI units of quantities used throughout this thesis.

Table 3.1: Physical units of important parameters used in nonlinear optics formulas and relations. Adapted from [3].

Physical Parameters		**SI units**
Intensity	I	$\mathrm{W/m^2}$
Fluence	F	$\mathrm{J/m^2}$
Power	P	W
Energy	ξ	J
Electric Field	E	V/m
Linear absorption coefficient	α_0	$\mathrm{m^{-1}}$
Nonlinear absorption coefficient	β	m/W
Linear refraction index	n_0	*dimensionless*
Nonlinear refraction index	γ	$\mathrm{m^2/W}$
Linear electric susceptibility	$\chi^{(1)}$	*dimensionless*
Third-order susceptibility	$\chi^{(3)}$	$\mathrm{m^2/V^2}$
n-order nonlinear susceptibilities	$\chi^{(n)}$	$(\mathrm{m/V})^{(n-1)}$
Wavelength	λ	m
Speed of Light	c	m/s
Vacuum Permitivity	ϵ_0	F/m

3.2 Linear and Nonlinear Optical Responses

Consider an electromagnetic wave with an electric field $E(t)$ passing through a medium. Let us describe the medium in a first approximation as a set of electric

temporal coherence.

dipoles, that is a dielectric medium. The electric dipoles are the two main opposite charges bounded by Coulomb forces that constitute the atom: the ion core (positive charge) and the electron (negative charge). The wave is carrying a perturbation to the medium as long as it propagates because the force exerted on the charges will have opposite signals. Consequently, a displacement of the electric dipoles from the mean position will be induced. When it happens, we say that the medium is polarized. Considered the electric dipoles' harmonic response:

$$m\left[\frac{dx^2}{d^2t}+\Gamma\frac{dx}{dt}-\omega_0^2x\right]=-eE(t), \tag{3.1}$$

where Γ is the damping constant, ω_0 is the resonance frequency and x is the displacement.

Imagine having two scenarios for an isotropic medium. Scenario (a): a "small" displacement of the electric dipoles caused by an applied field of intensity $3\,\mathrm{W/cm^2}$ from a yellow color LED[3]; Scenario (b): a "big" displacement because the reader decided to focus in the same electric medium a picosecond Nd:YAG mode-locked laser[4] consisting of an applied intensity of about $1\times10^{14}\,\mathrm{W/cm^2}$.

If the medium has a linear dielectric [26], scenario (a), the polarization $\overrightarrow{P}$ induced by the wave will be linearly proportional to the electric field, and assuming a transparent and isotropic medium, we have that

$$\vec{P}=\varepsilon_0\chi^{(1)}\vec{E}\,, \tag{3.2}$$

where ε_0 is the permittivity of the free space and $\chi^{(1)}$(dimensionless) is the linear susceptibility.

However, if the material is a nonlinear dielectric [26], scenario (b), a perturbation of the linear term occurs. Notice that the force applied in this case is closer to the Coulomb force, introducing nonlinearity and resulting in an anharmonic motion of electrons[5]. Therefore, in the equation of motion 3.1 the anharmonic terms need to be included. We can expand the polarization of the equation 3.2 in the following way [25]:

$$\vec{P}=\chi^{(1)}\vec{E}+\chi^{(2)}:\vec{E}\vec{E}+\chi^{(3)}\vdots\vec{E}\vec{E}\vec{E}+\ldots\ \text{higher order terms} \tag{3.3}$$

where $\chi^{(2)}$ and $\chi^{(3)}$ are the second- and third-order nonlinear optical susceptibilities, respectively. In equations 3.2 and 3.3 we considered that the fields $E(t)$ and $P(t)$

[3]Light Emission Diode

[4]Nd:YAG is the abbreviation for neodymium-doped yttrium aluminium garnet crystal ($\mathrm{Nd:Y_3Al_5O_{12}}$).

[5]The motion of the "heavier" nucleus is insignificant comparing to the much "lighter" electrons.

are vector quantities. In such a case, the susceptibilities $\chi^{(1)}$, $\chi^{(2)}$, ..., $\chi^{(n)}(n = 1, 2, 3, ...)$ become $(n+1)$th-rank tensors. However, throughout this thesis we will treat $E(t)$ and $P(t)$ as scalar quantities, so $\chi^{(1)}$, $\chi^{(2)}$, ..., $\chi^{(n)}$ will also be treated as scalares.

Until now, the usual nonlinear terms needed to characterized most of the NL optical effects rarely exceed $\chi^{(3)}$. We can ascend to a fifth-order nonlinear susceptibility $\chi^{(5)}$, for instance, when we are dealing with metamaterials or with plasmons. At a certain point, the evolution of the nth order of $\chi^{(n)}$ that was possible to achieve, described our science progress.

3.3 From Third-Order Susceptibility

If a material is centrosymmetric the phenomenon arising from the second-order optical nonlinearity $\chi^{(2)}$, will not be present. Thus the first nonlinear effects that take place in a nonlinear centrosymmetric material is arising from $\chi^{(3)}$. Because is out of the scope of this thesis, we will skipped the part of the second-order optical nonlinearity and the effects that are originated from it. For the reader who are interested we refer to the references [3, 24].

The Kerr lensing effect and the third-harmonic generation are example of phenomena arising from $\chi^{(3)}$(see equation 3.6). When a wave with enough intensity I propagates in materials with third-order nonlinearity, it is known that the optical index of refraction n, and the optical absorption coefficient α, are expressed as:

$$n = n_0 + \gamma I = n_0 + \frac{1}{2} n_2 |E|^2 \tag{3.4}$$

$$\alpha = \alpha_0 + \beta I = \alpha_0 + \alpha_2 |E|^2 \tag{3.5}$$

where γ and β are the nonlinear refraction index and the nonlinear absorption coefficient, respectively, n_0 is the linear refraction index and α_0 is the linear absorption coefficient. γ and β are associated since γ is proportional to the real part of the third-order susceptibility $\mathrm{Re}\,\chi^{(3)}$, while β is proportional to the imaginary part of the third-order susceptibility $\mathrm{Im}\,\chi^{(3)}$ through the following equations[6]:

$$\chi^{(3)} = \chi_R^{(3)} + i\chi_I^{(3)} \tag{3.6}$$

$$\chi_{\mathrm{I}}^{(3)} = \mathrm{Im}\chi^{(3)} = \frac{\beta\gamma^2\epsilon_0 c^2}{\omega} \tag{3.7}$$

[6]These equations are in S.I. units ($\mathrm{m}^2/\mathrm{V}^2$). To convert to esu units see for instance reference [27].

$$\chi_R^{(3)} = \mathrm{Re}\chi^{(3)} = 2\gamma\epsilon_0 c\, n_0^2 \tag{3.8}$$

where c is the speed of light in vacuum and ϵ_0 is the permittivity of free space.

3.3.1 Nonlinear Refraction and the Optical Kerr Effect

When we are under the conditions described in the previous section and we verify that equation 3.4 applies, we are in the presence of a Kerr-type nonlinear response. The phenomenon is called optical Kerr effect (OKE) or AC Kerr effect.

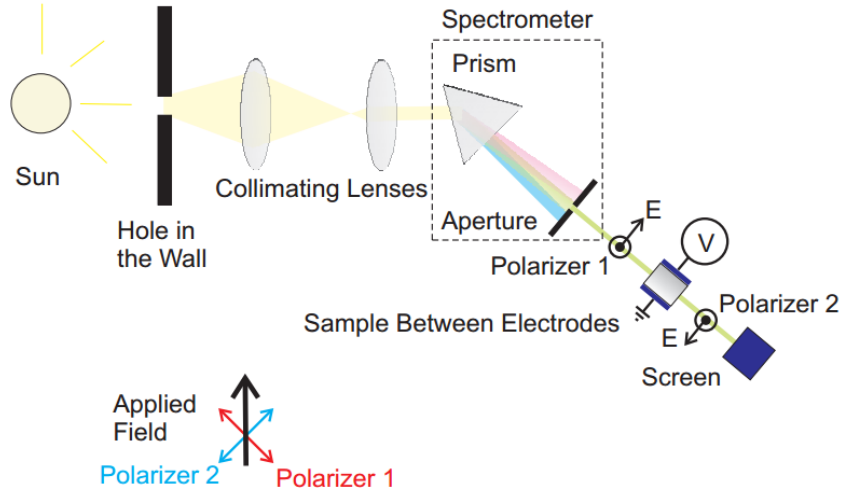

Figure 3.1: Diagram of the experiment through John Kerr (physicist, 1824-1907) founds a change in the refractive index of a plate of glass in the presence of an electric field. The effect was called electro-optic Kerr effect due to the presence of the applied electric field in the sample. The optical Kerr effect is essentially the same but it is due to "light itself", specifically due to the high intensity of the light source, so no Kerr cell is needed. Original from [2].

In OKE the intensity of light itself induces changes in the refraction index. That changes can lead to a self-focusing or self-defocusing behavior (see also section 4.2.1). In the self-focusing, the medium acts like a focusing lens causing a decrease in the beam radius. With the decreasing of the radius high optical intensities are reached and optical damaged may happen.

3.3.2 Nonlinear Absorption

One of the mechanisms that can be behind a nonlinear absorption is the two-photon absorption. It is a third-order nonlinear process that can be quantified by the parameter β. As the name indicates, two photons are simultaneously absorbed resulting in a excited state (see figure 3.2). This happens through a transient (virtual) state that

has an extremely small lifetime, i.e. on the order of a few femtoseconds (10^{-15}s). Until this virtual state is "alive" another photon (the second photon) can promote the particle to a highest level, otherwise it will decay.

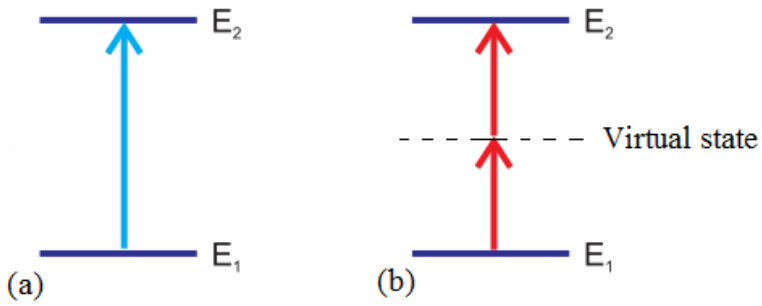

Figure 3.2: Two-photon absorption scheme. (a) Excitation involving one-photon absorption. (b) Excitation involving the interaction of two photons of half the energy. Adapted from [2].

Considering the time, the probability to observe a second absorption is very low. The intensity of the light source from an UV-visible spectrometer, for instance, is far from enough. In order to increase the probability very high intensities are needed (e.g. laser sources), enabling us to see the phenomena.

Chapter 4

Z-scan

4.1 Introduction

In the last chapter we saw that optical phenomena of our "everyday life" are regarded as properties of matter independent of the intensity of light. The importance and contribution of the intensity to the optical properties only became observable when lasers emerged, particularly pulsed lasers. Materials exposed to sufficiently high fields, as accessible with coherent light sources, can become nonlinear (see section3.2). They can exhibit either non-negligible nonlinear refraction (NLR) or/and nonlinear absorption (NLA) [22]. These processes can be quantified according to equations 3.4 and 3.5. Thus, a question arises. Suppose the reader is interested in these two processes (NLR and NLA) and wants to quantify them through the parameters of the equations mentioned. How can the reader measure them? One way is to use the Z-scan technique.

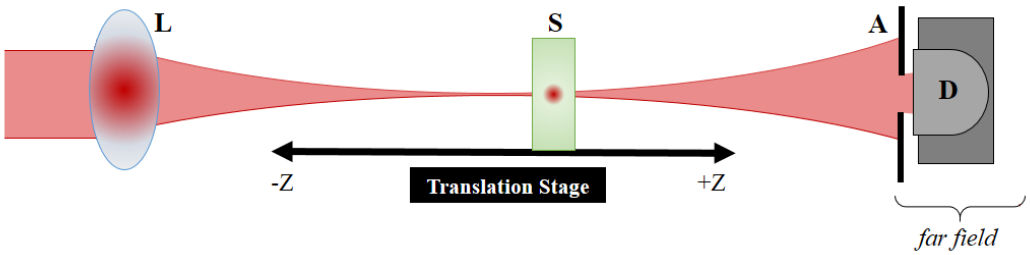

Figure 4.1: Simplified schematic for a Z-scan experiment (L - Focal Lens; S - Sample; A - Aperture; D - detector). The presence of A depends on the sample effect of interest. If A is present, Z-scan is in a close-aperture configuration and detects nonlinear refraction. In the absence of A, Z-scan is in an open-aperture configuration and detects nonlinear absorption.

Z-scan [28] was proposed by M. Sheik-Bahae *et al.* in 1989 [29] as an alternative technique[1] for the measurement of sign and magnitude of NLR index (γ) and NLA

[1]Different experimental techniques can be employed to measure n_2 and β, to say a few: nonlinear interferometry (1975); degenerate four-wave mixing (1987); ellipse rotation (1973); beam-

coefficient (β) using a single laser beam. As illustrated in figure 4.1, the sample is moved across the beam waist of a focused beam, through the direction of the beam propagation. The latter is called the z direction, hence the name Z-scan. Due to changes in spot size along the z-axis, the sample experiences different values of light intensity while moving. The resulting transmitted signal is detected in the *far field*[2] as a function of the sample position with respect to the focal plane (usually, $z = 0$ is defined at the focus). That signal is normalized often with respect to the linear transmittance response of the system (i.e. with respect to the transmittance values far from the focus), and plotted as a function of the z-position. Thus, it is possible to obtain the Z-scan curves that automatically tell us the sign[3] of n_2 or β.

The Z-scan basic setup can be divided into two configurations to determine n_2 and β separately. Regarded on the presence or absence of a finite aperture (i.e. a vertical slit or an iris [31]) aligned with the detector in the *far field*, we have (i) a close-aperture (CA) configuration or (ii) an open-aperture (OA) configuration[4], respectively. The CA is used for the study of NLR and the OA to study NLA[5].

In the next sections, we will cover the theoretical aspects behind Z-scan, some considerations on the NLR and NLA analysis, a Z-scan experimental viewpoint and a brief review of the technique applied to study of nonlinear optical properties of nanomaterials.

4.2 Basic Theory

Let us start by discussing the underlying theory of Z-scan. We will mainly be following references [28,29]. We refer the reader who seek a more detailed understanding or a different theoretical approach from what we present here to references [28] or [30], respectively.

Throughout the Z-scan experiment, the initial electric field undergoes two main changes. First, when it "hits" the sample and, secondly, when it passes through the

distortion measurements (1983). However, Z-scan itself is the most simple one in terms of setup apparatus.

[2]For this case in particular a distance of 10 Rayleigh lengths from the focus is a satisfactory approximation [30].

[3]i.e. self-focusing (positive n_2) or self-defocusing (negative n_2) phenomenon for nonlinear refraction. For the case of β a sign is not used. In that case the normalized transmittance increases or decreases.

[4]"Open-aperture" means that the entire beam that passed through the sample reaches the detector. In order to ensure that, sometimes the aperture is replaced by a lens to focus the beam in the detector.

[5]Notice that OA is insensitive to refraction, however the CA is sensitive to absorption. Because of that, if the NLA is present, it must be eliminated from the NLR response. Thus only remaining the effect from NLR. This is addressed in section 4.2.1.

final aperture[6], towards the detector. Consider an electric field $E(z, r, t)$ of a focused TEM_{00} Gaussian beam [32] traveling in the $+z$ direction (see figure 4.1) defined by:

$$E(z, r, t) = E_0(t)\,\frac{w_0}{w(z)} e^{-\varphi(r,z)} e^{-i\phi(z,t)} \tag{4.1}$$

where $E_0(t)$ contains the temporal envelope of the laser pulse and denotes the electric field at the focus, w_0 is the waist radius[7] at e^{-2}, $w^2(z)$ is the beam radius, $\varphi(r, z)$ is the radial phase given by

$$\varphi(r, z) = \left(\frac{r^2}{w^2(z)} + \frac{ikr^2}{2R(z)}\right), \tag{4.2}$$

and $\phi(z, t)$ is the temporal phase. The reader can find w_0 experimentally and calculate the remaining terms using the following expressions:

$$w^2(z) = w_0^2(1 + z^2/z_R^2), \tag{4.3}$$

$$R(z) = z(1 + z_R^2/z^2), \tag{4.4}$$

$$k = \frac{2\pi}{\lambda}, \tag{4.5}$$

where $R(z)$ is the radius of curvature of the wave front at z, k is the wave vector, λ is the laser wavelength and z_R is the Rayleigh length[8], given by:

$$z_R = \frac{\pi w_0^2}{\lambda}. \tag{4.6}$$

Let us now consider a "thin sample", that is, a sample with a length L much shorter than the Rayleigh length of the beam[9] ($L < z_R$). In other words, a sufficiently small light path $n_0 L$ so we can assume that the beam's diameter does not change throughout the sample.

Z-scan relies in the fact that the sample nonlinearity (see section 3.2) changes the electric field phase, which causes an amplitude distortion (spatial). To describe the electric field exiting the sample E_e, it is important to know how the amplitude and the phase of the electric field varies with the propagation depth z'.

[6] We are assuming a close-aperture configuration.
[7] i.e. The spot size at focus.
[8] Also known as Rayleigh range or diffraction length.
[9] To be more precise, L must be less than $z_R/\Delta\varphi(r = 0)$. Since $\Delta\varphi(r = 0)$ is most often small, $L < z_R$ is a sufficient criteria.

In expression 4.1 concerning the electric field, the term $e^{-i\phi(z,t)}$ contains the phase variation that is independent of r. Since we are only interested on the radial phase variation, we will omit the term $e^{-i\phi(z,t)}$ for now. Considering this aspect, the slowly varying envelope approximation (SVEA)[10] applies and can be used to simplify the calculations. Thus, the phase and amplitude of the electric field as a function of the propagation depth in the sample can be written as [28]:

$$\frac{d\Delta\phi}{dz'} = \Delta n(I)\, k \tag{4.7}$$

$$\frac{dI}{dz'} = -\alpha(I)\, I. \tag{4.8}$$

where $\Delta n = \gamma I$ (see equation 3.4) and $\alpha(I) = \alpha_0 + \beta I$ (see equation 3.5).

Solving these equations for the case of a cubic nonlinearity and negligible nonlinear absorption, we can find that the phase shift $\Delta\phi(z, r, t)$ at the end of the surface of the sample [29] is given by:

$$\Delta\phi(z, r, t) = \Delta\phi_0(z, r, t) \exp\left[-\frac{2r^2}{w^2(z)}\right] \tag{4.9}$$

where

$$\Delta\phi_0(z, t) = \left[\frac{\Delta\Phi_0(t)}{1 + z^2/z_0^2}\right]. \tag{4.10}$$

The term $\Delta\Phi_0(t)$ is the on-axis[11] phase shift and is defined as:

$$\Delta\Phi_0(t) = k\, \gamma I\, L_{eff}. \tag{4.11}$$

L_{eff} is the effective sample length, described by:

$$L_{eff} = (1 - e^{-\alpha L})/L. \tag{4.12}$$

This term is a correction factor for the linear absorption, assuming it exists at the measured wavelength. Otherwise, if the linear absorption is negligible, we consider $L_{eff} \simeq L$ [30].

We are able now to describe the electric field exiting the sample as:

$$E_e(z, r, t) = E(z, r, t)\, e^{\frac{-\alpha L}{2}} e^{i\Delta\phi(z,r,t)}. \tag{4.13}$$

[10] Brief, the approximation says that the variation of the amplitude A(z) with respect to z-axis is much smaller than the wavelength of the oscillation of the field [2]. Thus the SVEA (an the equations considering them) does not apply for few optical cycle pulses [31].

[11] Aperture centered on the optic axis.

Notice that the term $\exp(\frac{-\alpha L}{2})$ expresses the linear absorption phenomenon between light and sample, which leads to a decreasing electric field, and therefore, intensity.

The wave with electric field $E_e(z, r, t)$ will continue to propagate in the free space until it finds an aperture in the *far field*, where it will experience another change; but this time independent on z. Hence, the electric field pattern at the aperture, $E_a(r, t)$, can be described by [28]:

$$E_a(r,t) = E(z,0,t)\, e^{(\frac{-\alpha L}{2})} \sum_{m=0}^{\infty} \frac{[i\Delta\phi_0(z,t)]^m}{m!} \frac{w_{m0}}{w_m} e^{(-\varphi(r,z)+i\theta_m)}, \tag{4.14}$$

where

$$w_{m_0}^2 = \frac{w^2(z)}{2m+1}, \tag{4.15}$$

$$d_m = \frac{k w_{m_0}^2}{2}, \tag{4.16}$$

$$w_m^2 = w_{m_0}^2 \left[g^2 + \frac{d^2}{d_m^2} \right], \tag{4.17}$$

$$R_m = d \left[1 - \frac{g}{g^2 + d^2/d_m^2} \right]^{-1}, \tag{4.18}$$

$$\theta_m = tan^{-1} \left[\frac{d/d_m}{g} \right]. \tag{4.19}$$

This is a result which comes from the application of a "Gaussian decomposition" treatment . In short, the complex electric field was decompose into the summation of Gaussian beams through a Taylor series expansion of the nonlinear phase term.

Imagine now the case of nonexistence of an aperture in the *far field* (i.e. OA configuration).

With no aperture, Z-scan is insensitive to nonlinear refraction[12]. Thus, each change detected in transmission signal will arise from an absorption process. Moreover, it is expected the existence of a symmetric response with respect to the focus (e.g., at $z = 0$ we can have a minimum transmittance, thus a maximum absorption). Here, for the case of an open-aperture, we can think in a slightly different approach for the description of E_e. The nonlinear absorption reduces the irradiance $I_e(z, r, t)$ at the exit of the sample to an amount given by:

[12]Notice that we are considering a thin sample.

$$I_e(z,r,t) = \frac{I(z,r,t)e^{-\alpha L}}{1+q(z,r,t)}, \tag{4.20}$$

where $q = \beta\, I(z,r,t)\, L_{eff}$.

The nonlinear phase shift associated with $\Delta n = \gamma I$ is reduced by the nonlinear absorption of the beam:

$$\Delta\phi(z,r,t) = \frac{k\gamma}{\beta} len[1+q(z,r,t)]. \tag{4.21}$$

Combining these two equations, we obtain the complex field at the exit surface of the sample, which is:

$$E_e = E(z,r,t)e^{-\alpha L/2}(1+q)^{(\frac{ik\gamma}{\beta}-\frac{1}{2})}. \tag{4.22}$$

Finally, when E_a (in CA case, equation 4.14) or E_e(in OA case, equation 4.22) enter the detector, we will have a transmittance signal $T(z)$. With this signal we can experimentally extract the nonlinear coefficients β and n_2. For the sake of brevity, we will not go into details on how the transmittance function $T(z)$ is described in the cases of OA and CA. Instead, we will present in the following two sections the assumptions and main results for $T(z)$ in both cases, which are used in this work. We refer the reader who is interested in the demonstrations to one of the references given through this section.

During this chapter, we have been working with a Gaussian beam profile (spatial and temporal). However, in the literature there are other suitable descriptions for the case of a Z-scan performed with other laser profile types such top-hat or Lorentzian. As this is outside the scope of the thesis, we refer the readers to the reference [30].

4.2.1 Close Aperture

A representation of a purely[13] NLR Z-scan result is given in figure 4.2 for the two possible cases: a self-focusing medium or a self-defocusing medium (see section 3.3). The response function exhibits a peak (maximum in transmission) and a valley (minimum in transmission) as the sample is translated. How can we interpret this? Figure 4.3 can help us. Materials shows a lensing effect as a consequence of the increasing nonlinear refractive index, which leads to a sample causing a beam's divergence (therefore, thinking in terms of photons, less photons passing through the aperture) or a beam's convergence (more photons getting through the aperture).

[13] With no contribution from the NLA.

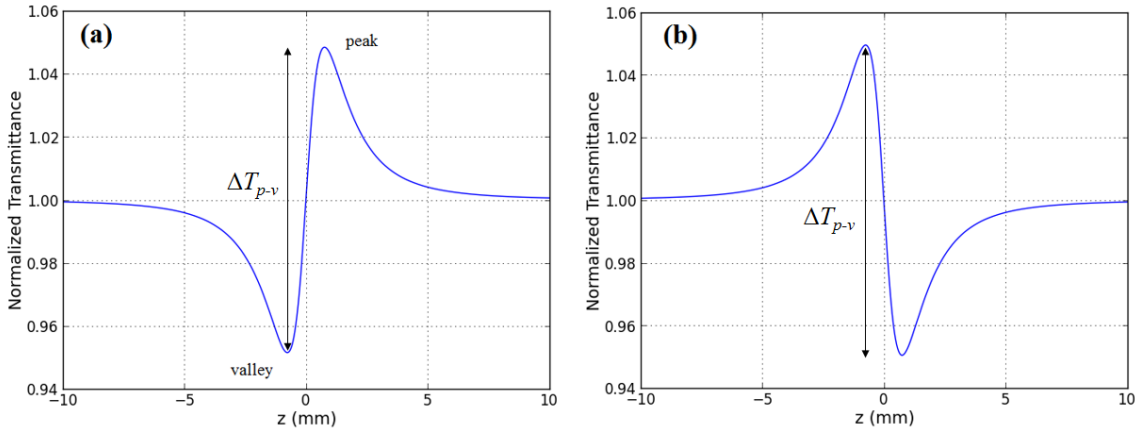

Figure 4.2: Z-scan nonlinear refraction response. (a) for a self-defocusing medium (i.e. negative n_2); (b) for a self-focusing medium (i.e positive n_2). n_2 can be estimated from the difference between the maximum (peak) and minimum (valley) values of the normalized transmittance, ΔT_{p-v}.

Consider the electric field at the aperture plane E_a given by equation 4.14. Let $E_a(z,\, r\, =\, 0,\, \Delta\phi_0)$ be the on-axis electric field. Then, if we assume (i) a cubic nonlinearity, (ii) a small phase change ($|\Delta\Phi_0| \ll 1$) and that (iii) the *far field* condition is satisfied ($d_{focus-detector} \gg z_R$), the normalized Z-scan transmittance can be approximated by [28]:

$$T(z, \Delta\Phi_0) \simeq 1 - \frac{4(z/z_R)}{[(z/z_R)^2 + 9]\ [(z/z_R)^2 + 1]}\Delta\Phi_0. \tag{4.23}$$

The peak and valley z-values of the Z-scan CA can be determined solving by

$$dT(z, \Delta\Phi_0)/dz = 0. \tag{4.24}$$

Inserting the two solutions into equation 4.23, we get for the peak and valley transmittance change ΔT_{p-v} (figure 4.2) the following approximation:

$$\Delta T_{p-v} \simeq 0.406\Delta\Phi_0. \tag{4.25}$$

Therefore, γ can be estimated from the phase shift $\Delta\Phi_0$ (see equation 4.11), which gives:

$$\gamma = \frac{\Delta T_{p-v}}{0.406\, k\, I_0\, L_{eff}}. \tag{4.26}$$

If, in the same conditions, the sample material shows NLR and NLA, then a contribution of the NLA to the NLR will be present while performing CA Z-scan measurements. Therefore, it needs to be eliminated! To obtain accurately measure-

ments for NLR it is always extremely important confirm the presence or absence of the NLA when performing in the CA scan. However, the opposite is not true. A possible suspicion that both phenomena are present, happens when the peak and valley from the NLR are not identical in magnitude [31]. Implementing $T_{CA(z)}/T_{OA(z)}$ before analyzing data enables us to determine correctly the nonlinear phase shift and, consequently, to estimate the NLR result.

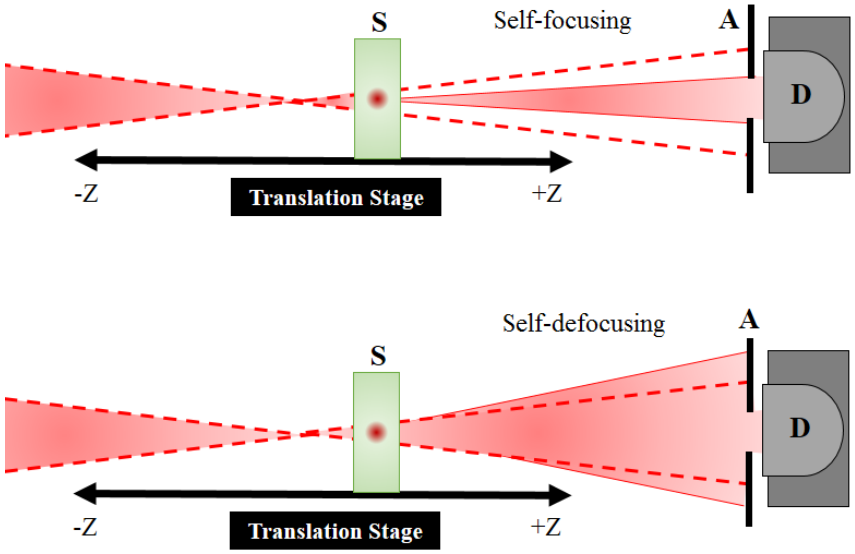

Figure 4.3: Representation of a self-focusing or defocusing phenomena during a CA Z-scan experiment. A - aperture; D - detector; S - sample.

4.2.2 Open Aperture

Direct multiphoton absorption, two-photon absorption, saturation of a single photon absorption[14], reverse saturable absorption or even dynamic free-carrier absorption [3,6,24,28] are different phenomena that can give rise to a NLA signal depending on the material characteristics and the experimental conditions (e.g. temporal resolution, intensity). Those phenomena leads to Z-scan traces either with a minimum transmittance valley (i.e. two-photon absorption) as in figure 4.4, or instead a maximum transmittance peak (saturable absorption). They occur at the focus.

Consider a two photon absorption process within the low excitation regime [28], where free carrier effects are neglected. Consider also the electric field E_e of equation 4.13. Solving equation 4.8, the irradiance distribution $I_e(z,r,t)$ at the exit surface of the sample can be written as

$$I_e(z,r,t) = \frac{I(z,r,t)e^{-\alpha L}}{1+q(z,r,t)} \tag{4.27}$$

[14] Also called saturable absorption.

where

$$q(z,r,t) = \frac{\beta I(z,r,t) L_{eff}}{1 + z^2/z_R^2}. \tag{4.28}$$

The transmittance $T(z)$ calculated through equation 4.27 gives[15] [28]:

$$T(z) = \frac{\ln\left[1 + q_0(z,t)\right]}{q_0(z,t)}, \tag{4.29}$$

where

$$q_0(z,t) = \frac{\beta I(t) L_{eff}}{1 + z^2/z_R^2}. \tag{4.30}$$

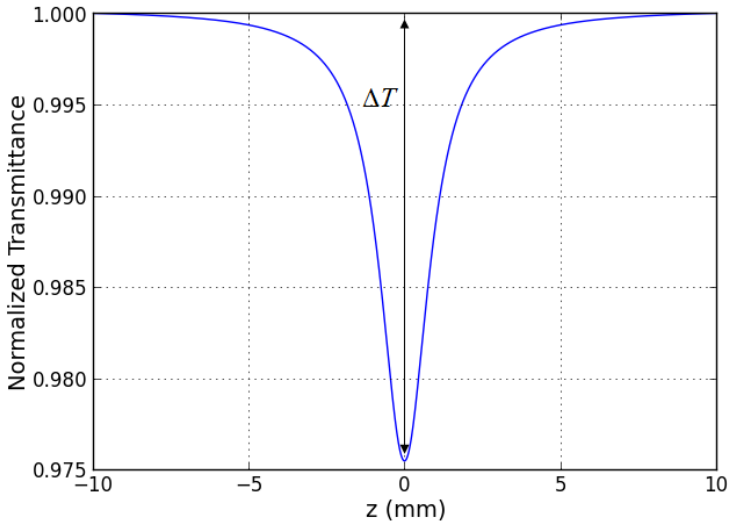

Figure 4.4: Example of a NLA response in a Z-scan experiment.

With equation, we can calculate the difference between the maximum and minimum values of transmission ΔT (see figure 4.4) . So, if we calculate them maximum of $T(z)$ for $z \to \infty$ and the minimum for $z = 0$ and then compute their difference, we get:

$$\Delta T = \left| 1 - \frac{\ln\left(1 + \beta I_0 L\right)}{\beta I_0 L_{eff}} \right|. \tag{4.31}$$

By knowing ΔT, I_0 and L_{eff}, we can extract the nonlinear coefficient β. Note that this does not allow us to perform fittings.

Assume now that $|q_0| < 1$. Since we are working with a temporally Gaussian

[15] This is done by obtaining the transmitted power $P(z,t)$ by integrating equation 4.27 at z over r. Then, a proper normalization of $P(z,t)$ gives $T(z)$. See reference [28] for more details.

pulse, we can write the transmittance $T(z)$ for the OA case as [28]:

$$T(z) = \sum_{m=0}^{\infty} \frac{[-q_0(z,0)]^m}{(m+1)^{3/2}} \tag{4.32}$$

This last expression is very useful for numerical calculations, i.e., for fitting experimental data.

4.3 Experimental Aspects

The beauty of Z-scan lies in its simplicity. Nevertheless, in practice, to take advantage of the Z-scan we need to pay careful attention to sources of errors. Efforts were and have been made to increase the technique sensitivity and to improve its usefulness [6, 30, 33]. Here, we pretend to discuss some experimental parameters of the Z-scan technique.

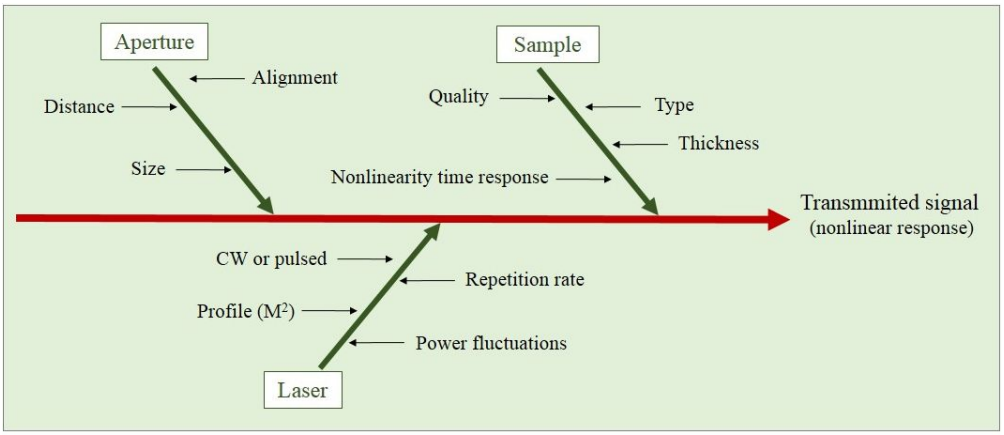

Figure 4.5: Some of the experimental aspects to consider while performing a Z-scan.

Beam parameters. Imagine that the reader is in doubt about the beam's parameters (e.g. spot size, w_0). Let us roughly call "calibration" as the process of testing the setup in order to obtain a result for a "standard sample" within an acceptable range. By standard sample we mean a nonlinear material with well known NLR and/or NLA response such as CS_2. It is possible to perform a Z-scan measurement and test if the beam parameters are correct in order to give the desired result for the well known nonlinear parameters β and n_2.

Apart from that, the temporal characteristics of the laser are one of the main important experimental aspects. A question arises: are there differences in the use of cw (continuous wave) lasers comparing with pulsed lasers? Are there advantages in performing a Z-scan with ultrashort laser pulses (ps or fs)? cw lasers are an

adequate option for the study of thermal nonlinearities (thermal lensing). However, when we are interested in the optical Kerr effect, using cw lasers may result in low precision measurements [30]. Phenomena as saturable absorption and reverse saturable absorption can be detected using a ns laser pulse, however, to detect two-photon absorption, higher temporal resolution is a requirement [5] (see section 3.3.2). Thus the study of two-photon absorption in materials by Z-scan requires a ps or fs regime.

Noise. Since Z-scan relies in the measurement of "intensity losses", intrinsic laser irradiance fluctuations can compromise the signal-to-noise ratio (S/N). To overcome that and improving the signal, most Z-scan schemes employ a reference arm consisting of a reference detector. This is important especially in the case of samples with weak nonlinear response, for monitoring the behavior of lasers with considerable instability (variations more than a few percent) - it helps to achieve a "cleaner" Z-scan trace.

Aperture. As we have seen, the aperture is a key-parameter in a Z-scan experiment. Its presence or absence determines what we are measuring (see section 4.1). Concerns about the aperture are mostly related with the accuracy of the NLR measurements. Two main aspects that experimentalists should take into account are the aperture alignment and size. Chapple et al. [30] addresses the impact of these aspects in Z-scan measurements.

4.4 Z-scan in Nanomaterials

Since we are able to tune the nanomaterials' optical properties they became a topic of great interest including and especially for nonlinear optics. Yet, a lot of work still need to be done. We next resume some investigations that used the Z-scan technique for the study of NLO properties of nanomaterials (including C-dots) within the last 10 years.

Vivacqua et al. [34] explored the nonlinear optical properties of a colloidal solution based on Fe_3O_4 magnetic nanoparticles with 10 nm diameter, using femtosecond laser pulses with frequencies between 100 Hz and 1 MHz. They obtained $\gamma = -(3.5 \pm 1.5) \times 10^{-14}\,\mathrm{cm}^2/\mathrm{W}$ and $\beta = (1.6 \pm 0.8)\,\mathrm{cm/GW}$ for frequencies up to $10^3\,\mathrm{Hz}$. Moreover, for pulse frequencies larger than $10^3\,\mathrm{Hz}$ they found that γ and β were increasing.

The NLA of colloidal platinum nanospheres protected by poly (N-vinyl-2-pyrrolidone) with 2 nm average diameter was investigated by Gao et al. [35]. They used a ns pulse Nd:YAG laser at 532 nm and a repetition rate of 1 Hz. They change the irradiance at

the focus from $1.1 \times 10^{11}\,\mathrm{W/m^2}$ to $6.5 \times 10^{11}\,\mathrm{W/m^2}$ and found a different behavior for the NLA. For the lower irradiances they found that the normalized transmission were increase at the focus, while for the highest irradiances the normalized transmittance decreases. The authors concluded that sample showed saturable absorption at lower intensities, while reverse saturable absorption at higher intensities.

Gordel et al. [36] submitted colloidal gold nanorods and colloidal gold nanoshells, both in water, to Z-scan studies. They used fs laser pulses over a broad range of wavelengths using an intensity at the focus ranging between 60 to 190 $\mathrm{GW/cm^2}$ and found a NL optical response (absorption and refraction) for both nanomaterials. They also found nanorods as the more efficient absorbers.

NL optical properties of a CdS colloidal solution were studied by Szeremeta et al. [37] in the wavelength range of 550-1600 nm and using fs laser pulses at 1 kHz. For a wavelength of 750 nm they found $\beta = 1.27 \times 10^{-9}\mathrm{cm/W}$ and $\gamma = 1.34 \times 10^{-14}\,\mathrm{cm^2/W}$. They compare their results with those of obtained from others authors in slightly different experimental conditions.

To the best of our knowledge the first publication about NL optical properties of carbon dots using the Z-scan technique was in 2013 with the work of Bourlinos et al. [4] with organophilic carbon dots prepared by pyrolysis of lauryl galate. For a concentration of 2.8 g/L they found $\chi^{(3)} = 160 \pm 10^{-13}\mathrm{esu}$. Aloukos et al. [5] studied the nonlinear optical response of some organophilic and hydrophilic carbon dots derived from gallate precursors. While Papagiannouli et al. [27] compared the NL optical response of nanodiamonds with the NLO response of the carbon dots under ns and ps laser pulses.

Chapter 5

Experimental Details

5.1 Overview

As it was mentioned, the work of this thesis consists of three parts (i) the synthesis of carbon dots and their characterization in terms of size, size distribution, and optical characteristics; (ii) the design and construction of a Z-scan setup; (iii) the study of the nonlinear optical properties of the C-dots using the Z-scan technique. In what follows we address the details of each part of the work.

5.2 Synthesis of Carbon Dots

The C-dots were prepared by one-step route based on the carbonization of ethylene glycol, which was adapted from [38]. 6 ml of ethylene glycol ($HOCH_2CH_2OH$) was added into 8.5 ml of concentrated sulfuric acid (H_2SO_4) under a vigorous stirring at approximately 80 °C. After 10 min, 15 ml of deionized water was added and the mixture was left cooling at room temperature ($\approx$ 23 °C). Then, the black precipitate was centrifuged two times at 6000 rpm during 15 min. The resulting supernatant was divided in two portions, one of them was additionally submitted to 15000 rpm during 15 min. Finally, the supernatant from the second centrifugation gave rise to the final product - a carbon dots aqueous colloidal dispersion. The ethylene glycol (99.5%) and concentrated sulfuric acid (95-97%) were purchased from Merck. The reagents were used without further purification.

5.3 Physicochemical Characterization Procedures

Molecular absorption (UV-Vis) spectroscopy and fluorescence spectroscopy (FLS) were performed at the Department of Chemistry and Biochemistry, University of Porto. The UV-Vis spectrum was collected with a Hewlett Packard 8452A diode array spectrophotometer in the 200—800 nm range using 1 cm path length quartz cuvette. The fluorescence excitation-emission spectrum were recorded with a Spex3D luminescence spectrophotometer equipped with a Xenon pulse discharge lamp (75 W)

and a CCD detector. The size of the slit was 5 mm and the integration time used was 1 s in an excitation wavelength range from 200 to 600 nm (step = 20 nm) and in an emission wavelength range from 200 to 800 nm (step = 5 nm) . The sample concentration was 3% (V/V). Transmission electron microscopy (TEM) was carried out in a Tecnai G2 20 FEI electron microscope, working at 180 kV, using low irradiation conditions (small spot size and low current). Images were acquired with a FEI Eagle CCD digital camera, at a resolution of 16 MP. A 3 μL drop of the C-dot sample was added into a carbon-formvar coated copper grid and left to dry overnight. Dr. Manuel Algarra from the University of Málaga was responsible for the TEM measurements performed at Centro Andaluz de Nanomedicina y Biotecnología (Málaga, Spain).

5.4 Z-scan Experiment

To study the optical nonlinearities of the C-dots aqueous solution, a Z-scan setup was built at the Laboratory for the Ultrafast Lasers and Magnetodynamic Spectroscopies at the Material Physics Institute of the University of Porto (IFIMUP-IN). The basic of a Z-scan setup was presented earlier in the section 4.1. As long as the principles and assumptions discussed are valid, it is possible to change the setup illustrated in figure 4.1. For instance, instead of using lenses, one can use mirrors to focus the beam on the sample.

We built a Z-scan setup that measures the transmitted light in a CA and in an OA configurations, simultaneously. A few-cycle ultrafast laser oscillator (Femtolasers Rainbow CEP), with a stable CEP, $\sim$ 7 fs, 81 MHz repetition rate and $\sim$ 2.5 nJ per pulse was used. As illustrated in figure 5.1, the beam is partial reflected by a glass wedge[1] of fused silica so that the power of the beam was reduced to $\sim$ 3 mW. After that, the beam goes through a biconvex lens (BK7 glass, 100 mm, Melles Griot) and it is focused on the C-dots aqueous dispersion (2.3 ± 0.3 g/L) in a quartz glass cuvette (1 mm optical path). The sample is free to move in the z-direction (i.e. throughout the beam waist) by a motorized platform (Zaber T-LSM050A, with a minimum step of 0.047625 μm) controlled by a computer. It is followed by a beam splitter (50%, p-polarized), where the beam splitting into two: the transmitted beam goes to the CA configuration and the reflect one goes to the OA configuration (see figure 5.2). In the former case, a mirror (protected silver, ThorLabs) changes the beams' direction towards a photodiode (ThorLabs

[1] The glass wedge is actually acting as a beam splitter. Initially, a BS was used, but we were not able to remove a second reflection from the second surface of BS.

PDB210A/M, with two detectors). Before reaching the photodiode the beam also passes through a biconvex lens (BK7 glass, 75 mm, Melles Griot). That happens to ensure that the entire beam passes through the photodiode's pinhole entrance. In the case of the transmitted beam, it passes by an iris (aperture diameter ≈2 mm) that is placed immediately before the photodiode. Therefore, just part of the this beam reaches the photodiode detector. A data acquisition (DAQ) device[2] was used to establish the connection between the computer and the photodiode.

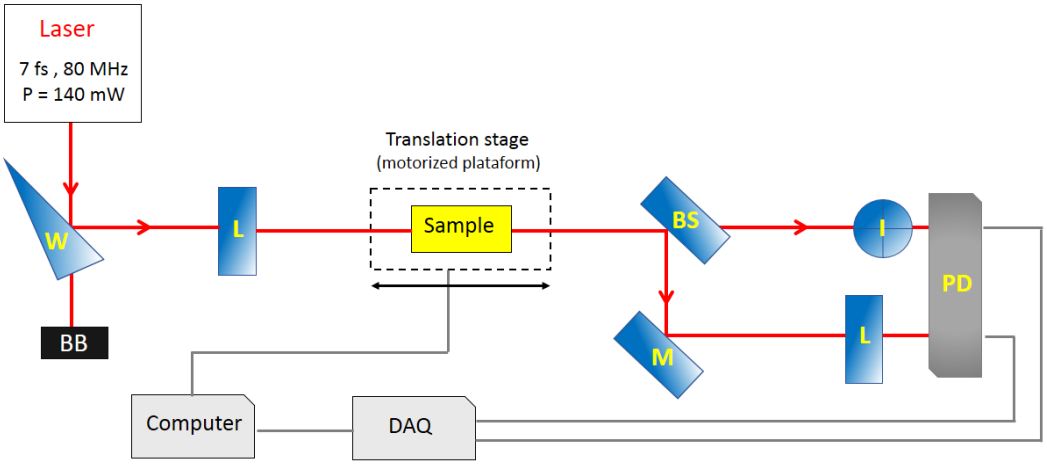

Figure 5.1: Z-scan setup: W - glass wedge; L - spherical lens; BS - beam splitter; M - mirror; I - iris; PD - photodiode; BB - beam blocker.

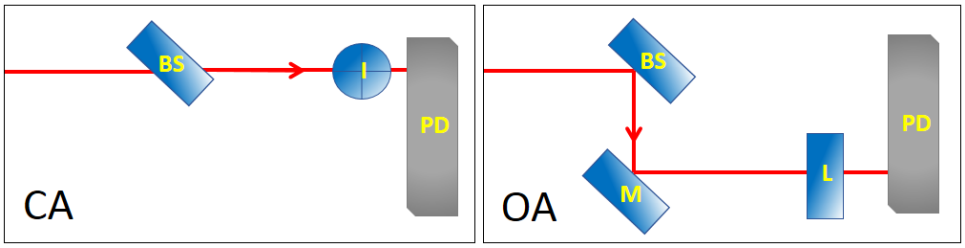

Figure 5.2: The two settings present at the end of Z-scan setup: a close-aperture (CA) for the measurement of n_2 and an open aperture (OA) for the measurement of β.

The laser spectrum was supervised daily before Z-scan measurements as the same as the power. The spectrum is in figure 5.3 and it was collected with a spectrometer (Ocean Optics HR4000). The value of the average wavelength is 827.9 nm.

[2]The GPIB interface of the lock-in (Stanford Research SR830) provided the DAQ

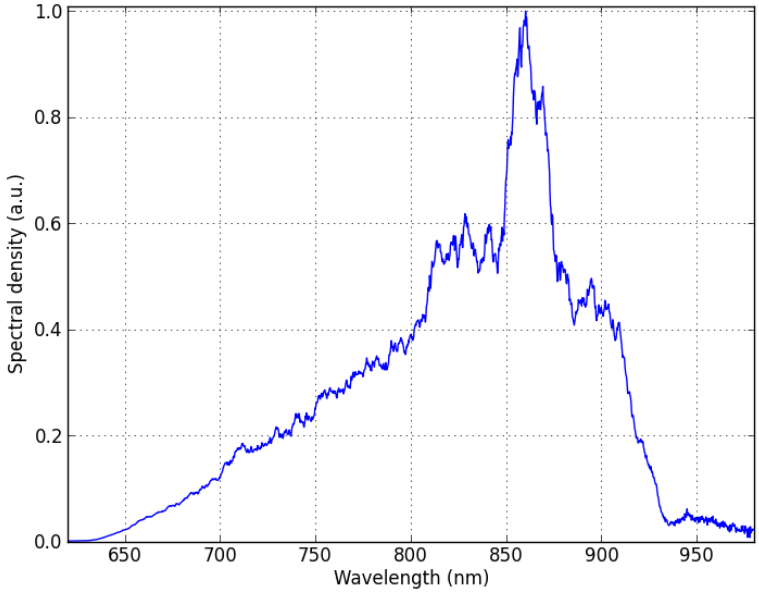

Figure 5.3: Ti:sapphire femtosecond laser spectrum.

A LabVIEW program was used to control the Z-scan experiment and acquire the Z-scan data. It was adapted from the original program designed by Tiago Magalhães to control a pump-probe setup [10]. Python scripts were made to treat and analyze the data from the Z-scan experimental and also from the PL measurements.

Chapter 6

Results and Discussion

6.1 Overview

We finally arrive to the chapter where we will be able to see what "optical secrets" are hiding in the C-dots synthesized and how they look like. Here, it will be shown and discussed the C-dots characteristics, namely, their diameter, size-distribution, linear absorption and luminescence properties. They were achieved through the use of the experiment described in section 5.4. The knowledge of the C-dots properties is interesting, not only from the fundamental point of view, but also because it enable us to predict their behavior and it is essential for a better understanding of where and how to use them. The size of a nanomaterial is perhaps a mandatory characteristic, making the microscopies like TEM essential and powerful tools within the area of nanomaterials. In the case of dots, the size is an important parameter since the optical properties are strongly dependent on their confinement (see section 2.1).

Apart from the "general" characteristics, the results of the nonlinear optical properties using a self-made Z-scan are also shown and discussed - achieving there results were the main objective of this work. The nonlinear optical properties mentioned are the third-order nonlinear refraction and nonlinear absorption described in section 3.3. The area of nonlinear optics applied to chemistry and material science is not new, since there are many works on the nonlinear optical measurements in solid-state and chemical species (see for example references [6, 25]). However, investigations of this kind using broadband ultrashort pulses is, as far as we know, an actual topic, as well as the study of the nonlinear properties of C-dots [5].

6.2 Characterization of the Carbon Dots

6.2.1 Morphology and Size Distribution

To find the shape, the mean diameter and the size distribution of the C-dots TEM images were acquired (see figure 6.1). As result, it was found that the colloidal

dispersed phase consists of an irregular but nearly spherical shaped C-dots with $4.5 \pm 0.1\,\text{nm}$ mean-diameter. The C-dots size distribution can be evaluated through the histogram presented in figure 6.1. The histogram is based on the size of 136 measured particles[1]. We can see that the diameter varies approximately in the range $[1.3 - 10.0]\,\text{nm}$. This interval is broader comparing with the reported by[2] Liu et al. [38] but it is a common size distribution within the literature for C-dots from colloidal dispersions, even synthesized from different procedures [14, 39].

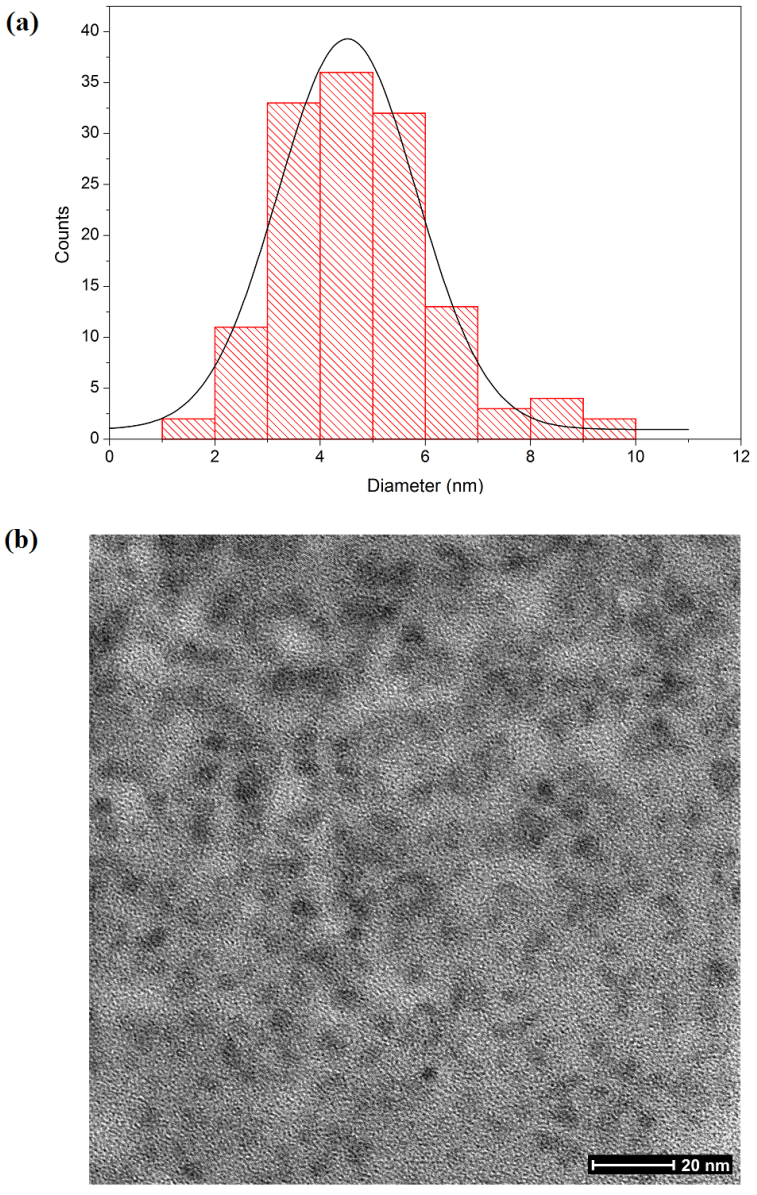

Figure 6.1: TEM results. (a) Histogram for the distribution of the diameter of C-dots dispersed in water expressed in terms of counts. (b) TEM image.

[1] The program ImageJ has been used for the purpose.
[2] Note that these are the same authors from which the basis of the C-dots synthesis was done.

Since the emission of light by *dots* is size dependent, the size distribution are strongly correlated with the excitation-emission spectrum, which will be discussed below. It is likely that more particles with a size less than 2 nm can be present in the aqueous dispersion, however, under the conditions used, it was difficult to detect and measure with a significant amount of certainty.

6.2.2 Linear Absorption and Fluorescence

The UV-vis absorption spectrum of the aqueous C-dots is presented in figure 6.2 and was obtained as described in section 5.3. It exhibits a significant absorption peak at 230 nm (5.39 eV) attributed to the $\pi \rightarrow \pi^*$transitions [14, 15, 38, 40]. This peak is expect in carbon dots [14, 38, 39] and graphene dots [15, 40] due to aromatic $C = C$ bonds. It is also perceptible a shoulder at around 300 nm (4.13 eV) ascribed to $n \rightarrow \pi^*$ transitions [38, 40], suggesting that the synthesized C-dots have oxygen-containing functional groups.

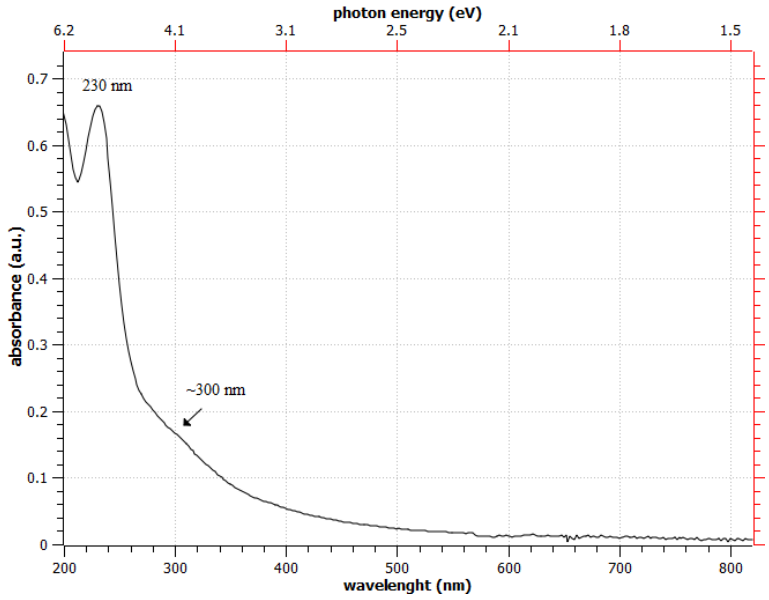

Figure 6.2: UV-visible spectrum of C-dots.

Our absorption results are in good agreement with the obtained by Y. Liu et al. [38] except we do not observe the broad absorption band at around 502 nm that is reported. The authors propose that this band can only be observed at very low pH values (pH<2). The UV-Vis sample analyzed here had a pH $\approx [2-3]$. The authors also report the IR and the XPS results of the C-dots from where they concluded the presence of carboxyl (-COOH) and hydroxyl groups (-OH). This leads us to believe in the existence of the same functional groups in the C-dots that were synthesized.

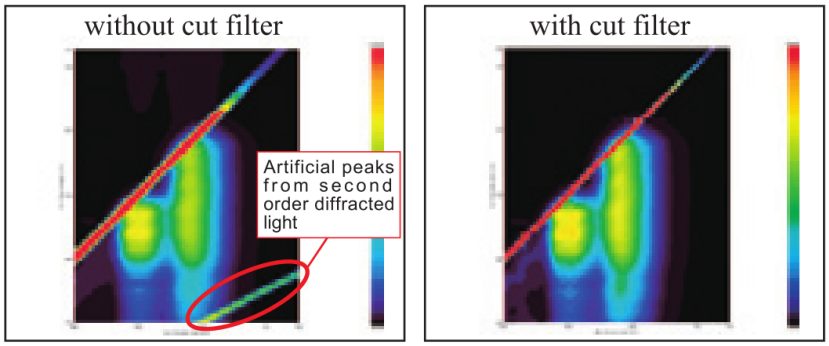

Figure 6.3: Illustration of the second order diffraction peaks that can while acquiring EEMs.

Some authors tried to extract the average diameter of quantum dots (as CdS and CdTe) from the linear absorption data - more precisely from the position of the absorption maximum [37, 41]. That estimation is done by applying the Brus model [41]. To the best of our knowledge, no one tried to do that for carbon based dots.

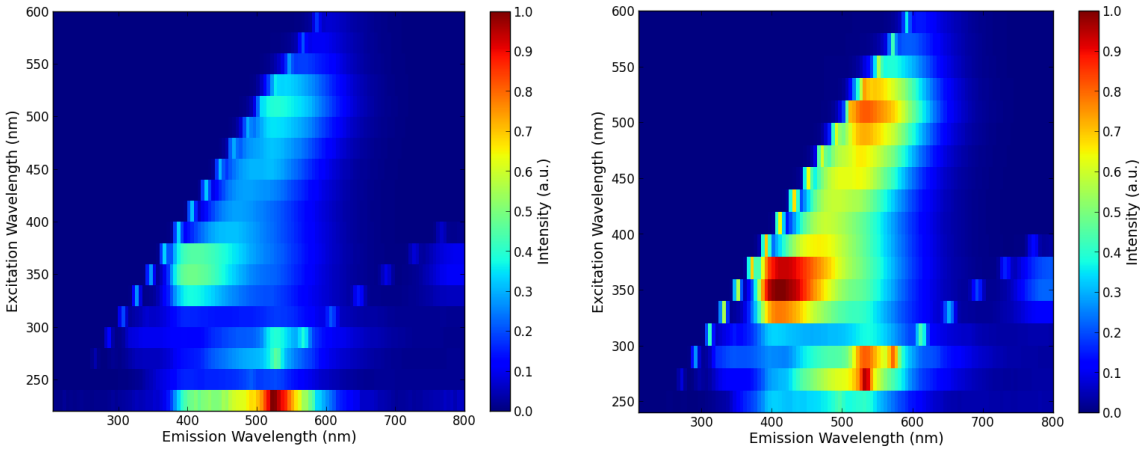

Figure 6.4: C-dots excitation-emission spectrum color map. (a) Results for excitation between 220 - 600 nm. (b) Results for excitation from 240 up to 600 nm.

Let us now discuss the fluorescence of the C-dots that was investigated from excitation-emission matrix (EEM) by FLS. The C-dots show wavelength-dependent luminescence (see figure 6.4). Due to the fact that no "cut filter" was used while acquiring the EEM, peaks due to high-order diffraction of light, caused by the excitation process, appear within the spectrum [42]. Thus, the peaks with no Gaussian behavior that appears in the EEM have nothing to do with the sample, it is just a question of light phenomenon (see figure 6.3). Hereupon, the emission lines for the wavelengths excitation 320 nm and 340 nm, which are represented in figure 6.5,

seem clearly composed by superposition of two Gaussian-like emission curves one centered at around 400 nm and other at around 510 nm. As long as we increase the wavelength excitation it can be observed a shift in the emission spectra to higher wavelengths (red-shift).

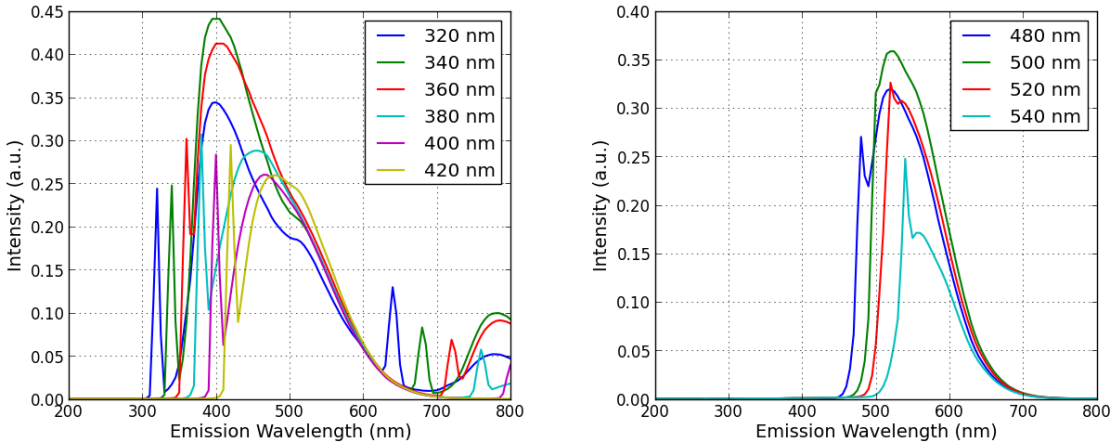

Figure 6.5: Emission spectra of C-dots in aqueous solution. (a) for excitation wavelengths between 320 and 420 nm; (b) for excitation wavelengths between 480 and 540 nm.

In figure 6.6, are the normalized results for the integrated intensity, i.e. the sum of the intensity values for each emission (figure 6.6 a) and excitation (figure 6.6 b). Through the results we can see that the light that is emitted by the C-dots has mostly a wavelength of 510 nm and the radiation that caused the highest excitation was 340 nm (in the interval [260-600] nm).

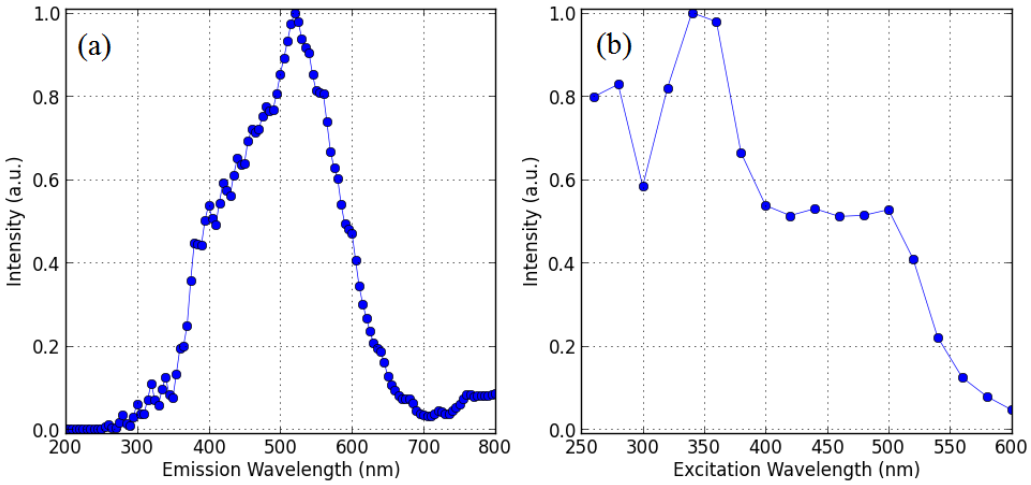

Figure 6.6: Integrated fluorescence response: (a) integrated excitation wavelength intensity for each emission wavelength; (b) integrated emission wavelength intensity as a function of the excitation wavelength (interval excitation values 260-600 nm).

6.3 Carbon Dots Nonlinear Optical Response

In the Z-scan setup depicted in figure 5.1 (see also the figure 8.1 in annex), five experiments were performed in order to extract the NLA and NLR transmission signal $T(z)$. The laser power immediately before the sample was 1.36 mW, the pulse duration was estimated to be[3] $\sim$ 74 fs, which gives an estimated peak intensity at focus of $I_0 \sim 50\,\mathrm{MW/cm^2}$. The waist size at the focus w_0 was estimated through fitting of equation 4.32 on the experimental data, which is of the order of the estimation done previously using a camera. Before performing measurements on the sample, we performed a Z-scan measurement on the quartz cuvette with water. No nonlinear response was found. Then, five experiments were performed in a row. The first measurement is illustrated in figure 6.7. Tables 6.1, 6.2 and 6.3 show the main results.

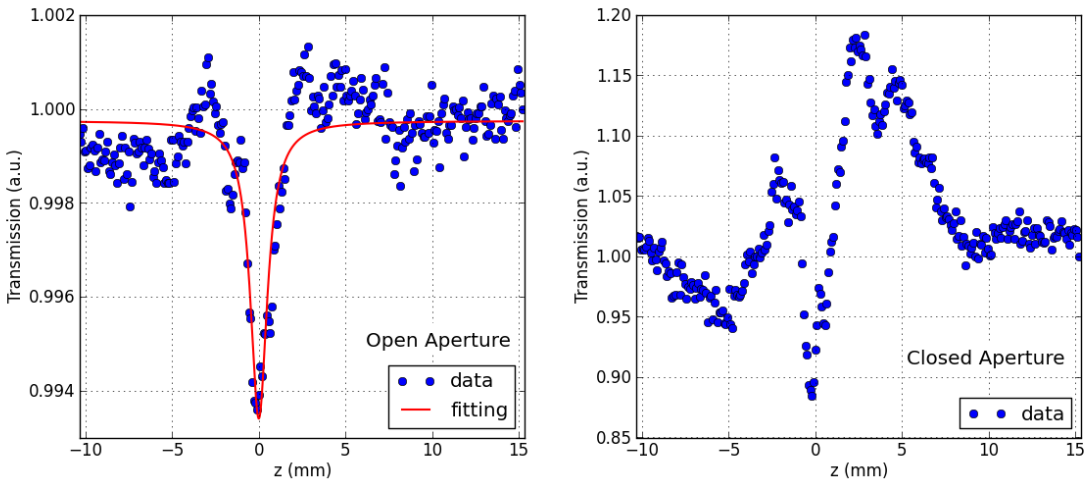

Figure 6.7: Z-scan results for the first measurement (see table 6.1). The transmission was normalized with respect to z far from the focus.

In our samples we observed a self-focusing behavior instead of the self-defocusing behavior reported so far for C-dots studied by Z-scan technique [4, 5, 27]. For instance, under 4 ns and 532 nm laser excitation Papagiannouli et al. [27] found $\gamma = -(9.8 \pm 1.5) \times 10^{-18}\mathrm{m^2/W}$ for a 2 g/L C-dot sample. In the case of the NLA, we observed a decrease in the transmission signal and $\beta \approx (2.6 \pm 0.2) \times 10^{-11}\mathrm{m/W}$. Depending on the initial excitation conditions and the sample concentration, it was reported previously cases of saturable absorption, reverse saturable absorption or even no detectable absorption signal [5].

[3] The pulse duration was estimated using the open-source software VirtualFemtolab, by Francisco Silva.

Table 6.1: Nonlinear absorption coefficient β of C-dots using a Ti:sapphire ultrafast oscillator (Femtolasers Rainbow CEP) at a repetition rate of 80 MHz, with a central wavelength of ~ 800 nm

Measurement	β (cm/GW)	$\overline{\beta}$ (cm/GW)	$\beta^{(*)}$ (cm/GW)	$\overline{\beta}^{(*)}$ (cm/GW)
A	3.9 ± 0.2	2.6 ± 0.2	2.7 ± 0.7	1.9 ± 0.5
B	2.5 ± 0.2		1.7 ± 0.4	
C	2.3 ± 0.2		2.3 ± 0.6	
D	2.2 ± 0.2		1.5 ± 0.4	
E	2.0 ± 0.2		1.5 ± 0.4	

(*) Computed through equation 4.31.

Table 6.2: Nonlinear refraction coefficient γ of C-dots using a Ti:sapphire ultrafast oscillator (Femtolasers Rainbow CEP) at a repetition rate of 80 MHz, with a central wavelength of ~ 800 nm. Computed through equation 4.25

Measurement	γ ($\times 10^{-17}$ m^2 W^{-1})	$\overline{\gamma}$ ($\times 10^{-17}$ m^2 W^{-1})
A	21 ± 5	17 ± 4
B	16 ± 4	
C	18 ± 5	
D	15 ± 4	
E	15 ± 4	

Table 6.3: Third-order nonlinear optical susceptibility $\chi^{(3)}$ of C-dots using a Ti:sapphire ultrafast oscillator (Femtolasers Rainbow CEP) at a repetition rate of 80 MHz, with a central wavelength of $\sim$ 800 nm. The values of β used are the ones computed through the fitting of equation 4.32.

Measurement	$\mathrm{Im}\chi^{(3)}$ ($\times 10^{-19}$m^2/V^2)	$\mathrm{Re}\,\chi^{(3)}$ ($\times 10^{-18}$m^2/V^2)	$\chi^{(3)}$ ($\times 10^{-18}$m^2/V^2)
A	2.37 ± 0.01	2.0 ± 0.5	2.0 ± 0.5
B	1.52 ± 0.01	1.5 ± 0.4	1.5 ± 0.5
C	1.40 ± 0.01	1.7 ± 0.5	1.7 ± 0.5
D	1.34 ± 0.01	1.4 ± 0.4	1.4 ± 0.5
E	1.22 ± 0.01	1.4 ± 0.4	1.4 ± 0.5

We found $\chi^{(3)} \approx (1.6 \pm 0.5) \times 10^{-18}$m^2/V^2 ($\approx 2 \times 10^{-11}$esu). Dividing by the sample concentration, C (g/L), we found $\chi^{(3)}/C \approx (7.0 \pm 0.3) \times 10^{-19}$m^{2}L/gV^2 ($\approx 9 \times 10^{-12}$esu L/g). Some of the values of $\chi^{(3)}/C$ reported so far for C-dots are $\chi^{(3)}/C = (2.6 \pm 0.2) \times 10^{-11}$esu L/g (under 35 ps, 532 nm and a concentration of 2

g/L) or $\chi^{(3)}/C = (0.6 \pm 0.1) \times 10^{-9}$esu L/g (under 4 ns, 532 nm and a concentration of 2 g/L) [27].

Finally, we think that our results from the CA Z-scan may have been affected by a misalignment of the setup.

Chapter 7

Conclusions and Future Work

A Z-scan setup was built capable of operating simultaneously in a close-aperture and open-aperture configurations. Hidrophilic green C-dots were synthesized from ethylene glycol. The synthesized C-dots in aqueous dispersion were found to exhibit a nonlinear optical response. Signals from the third-order nonlinear refraction and nonlinear absorption were detected using a Z-scan setup with a Ti:sapphire ultrafast oscillator (Femtolasers Rainbow CEP) at a repetition rate of 80 MHz, with a central wavelength of $\sim$ 800 nm. In particular, they exhibit self-focusing behavior and a large third-order nonlinear absorption response. This results provide new information about the nonlinear optical properties of carbon-dots in the near-infrared region. Moreover, the Z-scan setup that was built is able to measure optical nonlinearities from different materials, supporting new investigations using the technique with femtosecond broadband pulses. This thesis also aims to introduce those with different backgrounds and who are new in this subject, to Z-scan measurements.

As future work, several ideas can be considered. One of them, that could complement this study, is to determine the optical liming response of the C-dots by measuring the output fluence for different values of the input fluence. Another idea that can be explored is to try to perform Z-scan measurements with spectral resolution, i.e., use a spectrometer instead of a photodiode to take advantage of the broadband spectrum of the ultrafast laser.

Other possible ambitions are the following: (i) perform Z-scan measurements out of the SVEA regime by compressing the ultrashort pulses down to $\sim$ 7 fs, which is done with dispersion compensation; and (ii) study possible relations between the materials' properties (e.g. concentration and size of nanomaterials) and their third-order nonlinearity, which could be realized by individual studies or by implementing a chemometric experimental design.

Bibliography

[1] Edik U. Rafailov, editor. *The Physics and Engineering of Compact Quantum Dot-based Lasers for Biophotonics*. Wiley-VCH, 2014. xv, 6

[2] Mark G. Kuzyk. *Lecture Notes in Nonlinear Optics: A students perspective*. CreateSpace Independent Publishing Platform, 2013. xv, 15, 16, 20

[3] Richard L. Sutherland. *Handbook of Nonlinear Optics*. Marcel Dekker, 2nd, revised and expanded edition, 2003. xvii, 1, 12, 14, 24

[4] Athanasios B. Bourlinos, Michael A. Karakassides, Antonios Kouloumpis, Dimitrios Gournis, Aristides Bakandritsos, Irene Papagiannouli, Panagiotis Aloukos, Stelios Couris, Katerina Hola, Radek Zboril, Marta Krysmann, and Emmanuel P. Giannelis. Synthesis, characterization and non-linear optical response of organophilic carbon dots. *Carbon*, 61:640–649, 2013. 1, 28, 38

[5] Panagiotis Aloukos, Irini Papagiannouli, Athanasios B. Bourlinos, Radek Zboril, and Stelios Couris. Third-order nonlinear optical response and optical limiting of colloidal carbon dots. *Optical Society of America*, 22:12013–12027, 2014. 1, 27, 28, 33, 38

[6] Mark G. Kuzyk. *Characterization Techniques and Tabulations for Organic Nonlinear Materials*. Marcel Dekker, 1998. pag. 655-692. 1, 24, 26, 33

[7] S. V. Gaponenko. *Optical Properties of Semiconductor Nanocrystals*. Cambridge University Press, 1 edition, 1998. 3, 5

[8] Sheila N. Baker and Gary A. Baker. Luminescent carbon nanodots: Emergent nanolights. *Angewandte Chemie International Edition*, 49:6726–6744, 2010. 7, 8

[9] Riichiro Saito. *Physical Properties of Carbon Nanotubes*. Imperial College Press, 1998. 7

[10] Tiago Emanuel da Cunha Magalhães. Femtosecond pump-probe spectroscopy for studies of the ultrafast carrier dynamics in graphene. Master's thesis, Faculdade de Ciências da Universidade do Porto, 2014. 7, 32

[11] Leo Levi. *Applied Optics: A Guide to Optical System Design*, volume 1. 1968. 7

[12] Ya-Ping Sun, Bing Zhou, Yi Lin, Wei Wang, K. A. Shiral Fernando, Pankaj Pathak, Mohammed Jaouad Meziani, Barbara A. Harruff, Xin Wang, Haifang Wang, Pengju G. Luo, Hua Yang, Muhammet Erkan Kose, Bailin Chen, L. Monica Veca, and Su-Yuan Xie. Quantum-sized carbon dots for bright and colorful photoluminescence. *Journal of the American Chemical Society*, 128:7756–7757, 2006. 8

[13] Ping Yang, Ligang Zhou, Shenli Zhang, Neng Wan, Wei Pan, and Wenzhong Shen. Facile synthesis and photoluminescence mechanism of graphene quantum dots. *Journal of Applied Physics*, 116:1–7, 2014. 8

[14] Pyng Yu, Xiaoming Wen, Yon-Rui Toh, and Jau Tang. Temperature-dependent fluorescence in carbon dots. *Journal of Physical Chemistry C*, 116:25552–25557, 2012. 8, 34, 35

[15] Dengyu Pan, Jingchun Zhang, Zhen Li, and Minghong Wu. Hydrothermal route for cutting graphene sheets into blue-luminescent graphene quantum dots. *Advanced Materials*, 22:734–738, 2010. 8, 35

[16] Youxing Fang, Shaojun Guo, Dan Li, Chengzhou Zhu, Wen Ren, Saojun Dong, and Erkang Wang. Easy synthesis and imaging applicatiopns of cross-linked green fluorescent hollow carbon nanoparticles. *ACS Nano*, 6:400–409, 2012. 8

[17] Debasis Bera, Lei Qian, Teng-Kuan Tseng, and Paul H. Holloway. Quantum dots and their multimodal applications: A review. *Materials*, 3:2260–2345, 2010. 8

[18] Katerina Hola, Yu Zhang, Yu Wang, Emmanuel P. Giannelis, Radek Zboril, and Andrew L. Rogach. Carbon dots - emerging light emitters for bioimaging, cancer therapy and optoelectronics. *nanotoday*, 9:590–603, 2014. 8

[19] Vasilios Georgakilas, Jason A. Perman, Jiri Tucek, and Radek Zboril. Broad family of carbon nanoallotropes: Classification, chemistry and applications of fullerenes, carbon dots, nanotubes, graphene, nanodiamonds, and combined superstructures. *Chemical Reviews*, 115:4744–4822, 2015. 8

[20] Albrecht Rabenau. The role of hydrothermal synthesis in preparative chemistry. *Angewandte Chemie International Edition*, 24:1026–1040, 1985. 8

[21] P. A. Franken, A. E. Hill, C. W. Peters, and G. Weinreich. Generation of optical harmonics. *Physical Review Letters*, 7:118–119, 1961. 12

[22] Paul N. Butcher and David Cotter. *The Elements of Nonlinear Optics*. Cambridge University Press, 1991. 12, 17

[23] Joseph H. Simmons and Kelly S. Potter. *Optical Materials*. Academic Press, 2000. 12

[24] Robert W. Boyd. *Nonlinear Optics*. Academic Press, 3 edition, 2008. 12, 14, 24

[25] Paras N. Prasad. Is there a role for organic materials chemistry in nonlinear optics and photonics? *Chemistry of Materials*, 2:660–669, 1990. 12, 13, 33

[26] E. T. Jaynes. Nonlinear dielectrics. *Proceedings of the I.R.E.*, 43:1733–1737, 1955. Jaynes1995. 13

[27] Irene Papagiannouli, Athanasios B. Bourlinos, Aristides Bakandritsos, and Stelios Couris. Nonlinear optical properties of colloidal carbon nanoparticles: nanodiamonds and carbon dots. *RSC Advances*, 4:40152–40160, 2014. 14, 28, 38, 40

[28] M. Sheik-Bahae, A. A. Said, T. H. Wei, D. J. Hagan, and E. W. Van Stryland. Sensitive measurement of optical nonlinearities using a single beam. *IEEE Journal of Quantum Electronics*, 26:760–769, 1990. 17, 18, 20, 21, 23, 24, 25, 26

[29] M. Sheik-Bahae, A. Said, and E. W. Van Stryland. High-sentitivity single-beam n2 measurements. *Optics Letters*, 14:955–957, September 1989. 17, 18, 20

[30] P. B. Chapple, J. Staromlynska, J. A. Hermann, T. J. Mckay, and R. G. Mcduff. Single-beam z-scan: Measurement techniques and analysis. *Journal of Nonlinear Optical Physics and Materials*, 6:251–293, 1997. 18, 20, 22, 26, 27

[31] Technology and Applications Center Newport Corporation. *Z-Scan for the Characterization of Transparent Optical Materials*, 2007. 18, 20, 24

[32] Sidney A. Self. Focusing of spherical gaussian beams. *Applied Optics*, 22:658–661, 1985. 19

[33] Jean-Michel Ménard, Markus Betz, Iliya Sigal, and Henry M. van Driel. Single-beam differential z-scan technique. *Applied Optics*, 46:2119–2122, 2007. 26

[34] D. Espinosa M. Vivacqua and A. M. F. Neto. Application of the z-scan technique to determine the optical kerr coefficient and two-photon absorption coefficient of magnetite nanoparticles colloidal suspension. *Journal of Applied Physics*, 111:1–5, 2012. 27

[35] Yachen Gao, Xueru Zhang, Yuliang Li, Hanfan Liu, Yuxiao Wang, Qing Chang, Weiyan Jiao, and Yinglin Song. Saturable absorption and reverse saturable absorption in platinum nanoparticles. *Optics Communications*, 251:429–433, 2005. 27

[36] Marta Gordel, Radoslaw Kolkowski, Joanna Olesiak-Banska, Katarzyna Matczyszyn, Malcolm Buckle, and Marek Samo'c. Z-scan studies of nonlinear optical properties of colloidal gold nanorods and nanoshells. *Journal of Nanophotonics*, 9:1–11, 2015. 28

[37] Janusz Szeremeta, Marcin Nyk, Dominika Wawrzynczyk, and Marek Samoc. Wavelength dependence of nonlinear optical properties of colloidal cds quantum dots. *Nanoscale*, 5:2388–2393, 2013. 28, 36

[38] C.-y. Liu Y. Liu and Z. y. Zhang. Graphitized carbon dots emitting strong green photoluminescence. *Journal of Materials Chemistry C*, 1:4902–4907, 2013. 29, 34, 35

[39] Lei Wang, Shou-Jun Zhu, Hai-Yu Wang, Song-Nan Qu, Yong-Lai Zhang, Jun-Hu Zhang, Qi-Dai Chen, Huai-Liang Xu, Wei Han, Bai Yang, and Hong-Bo Sun. Common origin of green luminescence in carbon nanodots and graphene quantum dots. *ACS Nano*, 8:2541–2547, 2014. 34, 35

[40] Xiaoming Wen, Pyng Yu, Yon-Rui Toh, Xiaoqian Ma, and Jau Tang. On the upconversion fluorescence in carbon nanodots and graphene quantum dots. *Chemical Communications*, 50:4703–4706, 2014. 35

[41] W. William Yu, Lianhua Qu, Wenzhuo Guo, and Xiaogang Peng. Experimental determination of the extinction coefficient of cdte, cdse, and cds nanocrystals. *Chemistry of Materials*, 15:2854–2860, 2003. 36

[42] *FP-8000 Series Spectrofluorometer Jasco Manual*. 36

Chapter 8

Annex

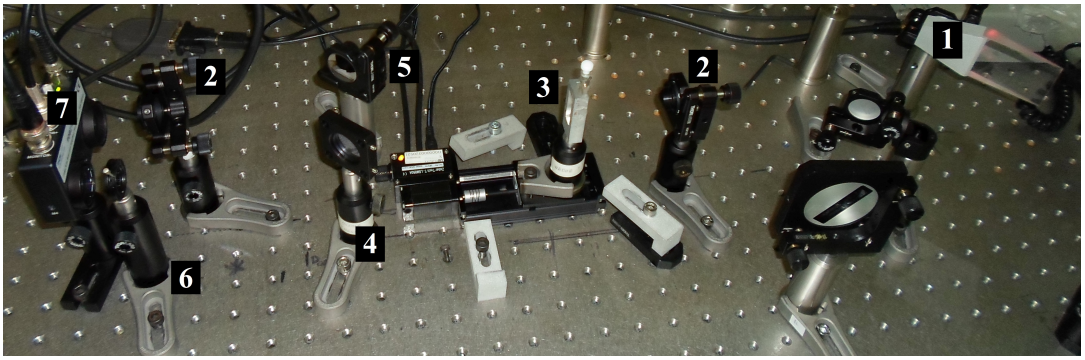

Figure 8.1: Z-scan setup. 1 - Wedge; 2 - Focal Lenses; 3 - Sample in a motorized platform stage; 4 - Beam Splitter; 5 - Silver Mirror; 6 - Iris; 7 - Photodiode.

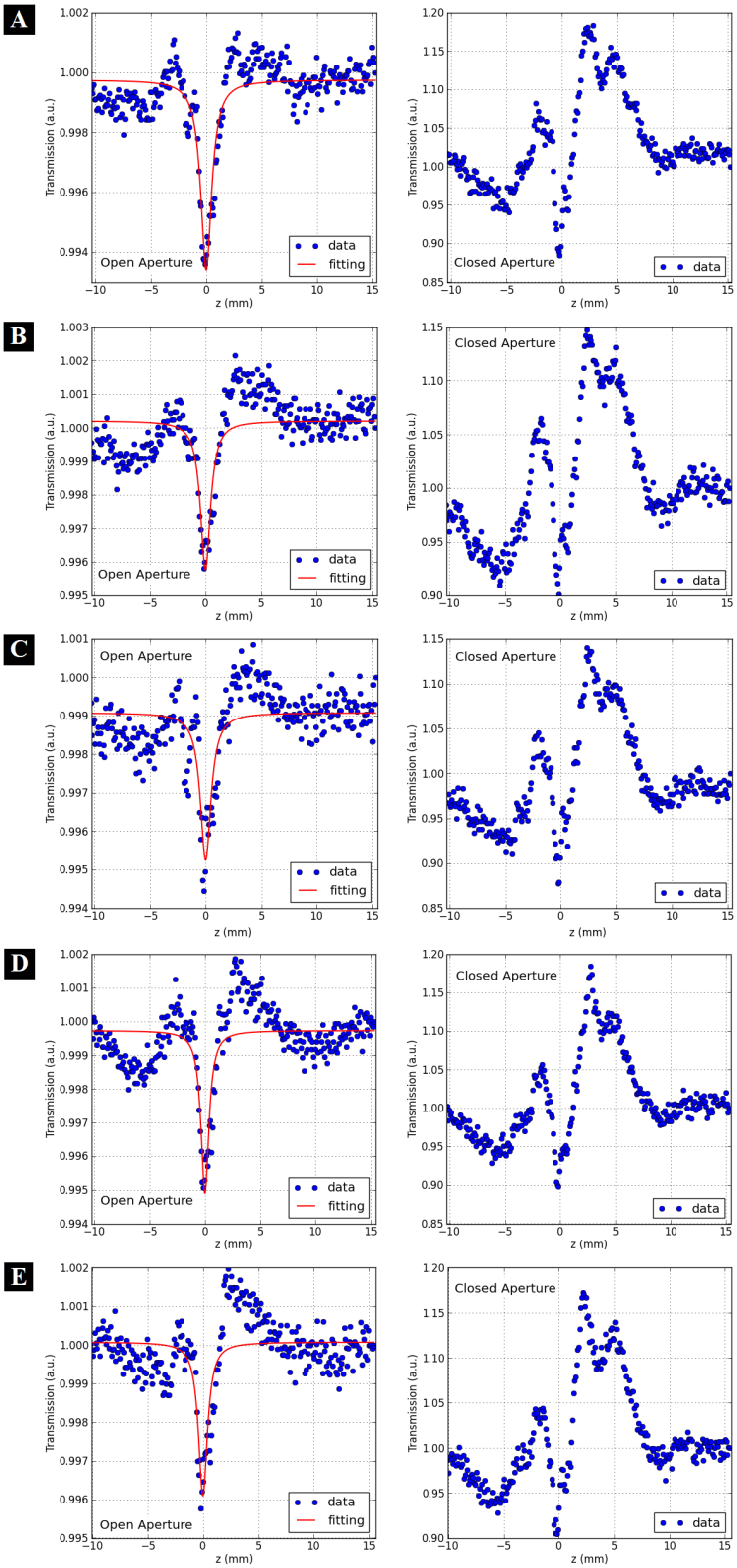

Figure 8.2: Z-scan transmittance of the five measurements from 6.3. Measurements in conditions of repetibility.